SAHARAN AIR LAYER INFLUENCES ON PUERTO RICO HYDROLOGICAL RESPONSE

by

SHELBY RINITA INGRAM

(Under the Direction of Thomas Mote)

ABSTRACT

The limited groundwater capacity of Puerto Rico makes rainfall critically important. In the past, rainfall perturbations for the island led to droughts that resulted in water rationing and threatened the biodiversity of the island's tropical rainforest in the Luquillo Mountains. Rainfall suppression can occur during the early rainfall season (ERS) from Saharan Air Layer influences on thermodynamics. Global Climate Models (GCM) predict droughts to continue but are too coarse to provide a regional analysis for Puerto Rico. GCM output from European Centre for Medium-Range Weather Forecasts Reanalysis v5 (ERA5) and Coupled Model Intercomparison Project Phase 5 (CMIP5) were dynamically downscaled with the Weather Research and Forecasting Model. Analysis periods consisted of a historical period from 2014–2018 and future periods from 2045–2049 and 2085–2089. Future aerosol measurements and atmospheric patterns support longer dust intrusions into the Caribbean. In the Luquillo Mountains, between the historical and end-century periods ERS rainfall decreases significantly with (80%) and without (63%) dust. The most significant declines occur by the end of the mid-century. Similarly, convective potential decreases, but May and June remain the most convective months of the dust season.

INDEX WORDS: Puerto Rico, Saharan Air Layer, Weather Research and Forecasting Model, Dust, Drought, Rainfall, Early Rainfall Season

SAHARAN AIR LAYER INFLUENCES ON PUERTO RICO HYDROLOGICAL RESPONSE

by

SHELBY RINITA INGRAM

BS, The University of North Carolina at Asheville, 2018

A Thesis Submitted to the Graduate Faculty of The University of Georgia in Partial Fulfillment of the Requirements for the Degree

MASTER OF SCIENCE

ATHENS, GEORGIA

2022

SAHARAN AIR LAYER INFLUENCES ON PUERTO RICO HYDROLOGICAL RESPONSE

by

SHELBY RINITA INGRAM

Major Professor:	Thomas Mote
Committee:	Marcus Williams
	J. Marshall Shepherd
	Marguerite Madden

Electronic Version Approved:

Ron Walcott
Vice Provost for Graduate Education and Dean of the Graduate School
The University of Georgia
December 2022

DEDICATION

This thesis is first and foremost dedicated to my grandmothers, who passed prior to me completing this work but instilled the confidence, courage, and determination in me that I've needed to reach this goal. None of this would have been possible without my mom's insight to see my love for weather at a young age. Without her dedication to finding programs for me to participate in related to the field, my educational development would not have been the same. To my husband, your commitment to allowing my dreams to be our dreams receives all my gratitude. Our family will forever be my inspiration to keep aspiring to be the best I can be.

ACKNOWLEDGEMENTS

Thank you to my parents, siblings, family, and friends that have always been excited to support their favorite meteorologist without limits. To my husband, Issac Saxon, thank you for your countless hours of assistance. From helping me with presentations to making sure I took meaningful work breaks - nothing was unnoticed. I would like to especially acknowledge Dr. Thomas Mote, for always speaking positive affirmations into me and providing me with an invaluable educational experience. I admire your personal and educational transparency and ability to make all your students feel valued and supported in all our goals and achievements. The models conducted in this work would not have been possible without Dr. Paul Miller. Thank you for leading these simulations and providing Python code to post-process the model output. I also want to acknowledge my committee members, Drs. Marcus Williams, Marguerite Madden, and J. Marshall Shepherd for their guidance throughout this process. A special thank you to Dr. Williams for helping me set up, conduct, and analyze my model simulations. Lastly, I would like to thank all my educators from grade school, Charlotte Flights Track Club and the many internships and science programs that I have had the pleasure of being a part of.

TABLE OF CONTENTS

Page

LIST OF TABLES

Page

LIST OF FIGURES

Page

CHAPTER 1

Introduction

Puerto Rico is the smallest island of the Greater Antilles, with a land area of about 9,100 km^2 (Gómez-Gómez et al., 2014). The Puerto Rico archipelago, located between latitudes 17.58º N and 18.32º N, and longitudes 65.15º W and 68.00º W, consists of the main island and three smaller islands. Island topography mainly consists of alluvial deposits along coastal lowlands and a mountainous interior (Fig. 1). Mountain chains in the interior span almost the entirety of the island from east to west. In the northeast, the Luquillo Mountains feature the only remaining tropical rainforest on the island, critical ecological species, and the headwater of nine major rivers (Gómez-Gómez et al., 2014; Zinnert et al., 2021). The topography of the Luquillo Mountains and the orientation relative to the trade winds result in the highest mean annual precipitation on the island.

Precipitation in Puerto Rico has a seasonal pattern with two distinct maxima. Any regional and global weather and climate variability, including rainfall, strongly influences the Luquillo Mountains' biological dynamics (Waide et al., 2013; Zinnert et al., 2021). For example, during the early rainfall season (ERS) of 2015, the Luquillo mountains received about 50% of its 1985–2014 climatological average rainfall (Mote et al., 2017). The reduced rainfall resulted in visible declines in streamflow and soil and vegetation health within and downstream from Luquillo (NOAA NCEI, 2016; Zinnert et al., 2021). Global climate models (GCMs) predict future precipitation reductions and increases in drought in the tropics (Hartmann et al., 2013; Zhao & Dai, 2015; Herrera & Ault, 2017). These predictions and evidence from the 2015

drought have galvanized drought research at the Luquillo Long-Term Ecological Research site (LUQ LTER).

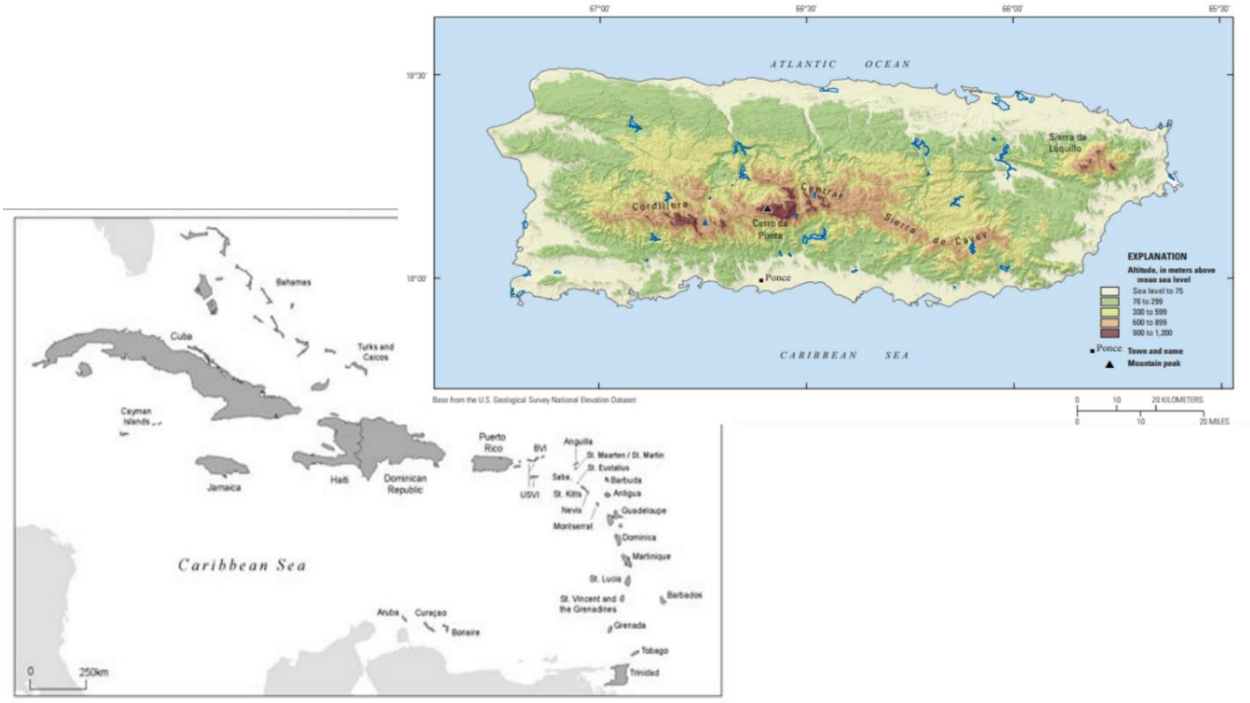

Figure 1. Puerto Rico is located within the insular Caribbean. The central and northeast portion of the island features the Luquillo and Cordillera Central mountains.

The LUQ LTER was established by the National Science Foundation in 1988 to study the long-term effects of anthropogenic and natural disturbances. As a part of the LUQ LTER effort, Mote et al. (2017) noted the role of early intrusions of the Saharan dust in the 2015 drought, and Miller et al. (2019) sought to understand the Saharan Air Layer (SAL) role in inhibiting precipitation over Puerto Rico. The SAL is a dry, hot air layer that extends from about 550 to

850 hPa due to desert dust outbreaks that inhibit rainfall (Dunion, 2011). This thesis investigated the role of global climate change on the temporal extent of the SAL over Puerto Rico. More specifically, the following questions were explored:

- How will the dust intrusion period be affected by anthropogenic warming of the oceans in the Tropical Atlantic?
- How does the seasonality and duration of dust intrusion affect water resources in Puerto Rico, specifically the Luquillo Mountains?

To address these questions, a regional numerical model, the Weather Research and Forecasting Model (WRF), was used to simulate historical and future atmospheric conditions over Puerto Rico. GCM output is readily available for future periods with various forcings. To represent a warmer climate from anthropogenic and natural variability, representative concentration pathway (RCP) 8.5 models were employed for the future simulations. The model was run at a coarse resolution and dynamically downscaled to a higher resolution. Chapter 2 provides a summary of previous literature on the questions posed above, while Chapters 3 and 4 explain the research design and data. Chapter 5 outlines findings with further discussion and conclusions in Chapters 6 and 7.

CHAPTER 2

Background

2.1 Mechanisms for Caribbean Precipitation Variability

Precipitation variability throughout Puerto Rico and the Caribbean is influenced by several characteristics at differing spatial and temporal scales. Puerto Rico precipitation exhibits a bimodal distribution, with two wet periods from late March through May and August through November (Gamble & Curtis, 2008). The dry season typically begins in December and lasts through mid-March. The secondary wet season is partially associated with tropical storms, while the dry season features cooler sea surface temperatures and high wind shear (Gamble & Curtis, 2008; Ramseyer & Mote, 2017). Most of the Caribbean experiences a decrease in rainfall during June and July, known as the mid-summer drought (MSD). The MSD is mainly influenced by an expansion and intensification of the North Atlantic Subtropical High (NASH). The dryness during this period is expected to intensify through the 21st century (Ramseyer & Mote, 2017). The MSD in Puerto Rico is not as pronounced as in other Caribbean islands, but there is a slight decline in the annual precipitation cycle signal during this period (Chen & Taylor, 2002; Gamble & Curtis, 2008; Angeles et al., 2010).

In 1994 and 2015, Puerto Rico experienced abnormally low rainfall, resulting in decreased water availability for agricultural and ecological activities (Larsen, 2000; NOAA NCEI, 2016; Schwartz et al., 2019). The warm phase of the El Nino-Southern Oscillation (ENSO) and the positive phase of the North Atlantic Oscillation (NAO) are associated with drier-than-normal conditions for the Caribbean (Malmgren et al., 1998; Giannini et al., 2000;

Jury et al., 2007). The ENSO warm phase, commonly known as El Nino, is associated with positive sea surface temperature (SST) anomalies in the Pacific, resulting in a dry atmosphere in the Caribbean (Trenberth, 1997). The NAO is a measure of a dipole of atmospheric mass anomalies in the tropical and North Atlantic, with one form calculated from the sea level pressure difference between the Azores high and Icelandic Low (Charlery et al., 2006; Jury et al., 2007).

Additional factors such as tropical cyclones, regional and local wind patterns, and dust aerosols have been shown to interrupt the bi-modal precipitation pattern for the region (Angeles et al., 2010; Ashby et al., 2005). The Caribbean's location downwind of the Saharan desert makes the area a dust sink (Prospero & Mayol-Bracero, 2013). Doherty et al. (2008) and Prospero and Mayol-Bracero (2013) found an increase in Sahel dust emission and Caribbean aerosol optical depth (AOD) since the early 1970s. Additionally, there is strong evidence that desert dust emissions are sensitive to the climate (Prospero & Lamb, 2003; Mahowald et al., 2010). Dusty periods have been related to glacial erosion, increased dust source area extent, soil dryness, and differential surface heating that influence emission conducive wind patterns (Kohfeld & Harrison, 2001; Albani & Mahowald, 2019). Nevertheless, there remain numerous unknowns regarding how Saharan dust will impact precipitation climatology in the future (Mahowald et al., 2010; Albani & Mahowald, 2019).

2.2 Dust Interactions

Mobilized desert dust can remain in the atmosphere for at least a week (Gioda et al., 2013; Reid et al., 2002; Shao et al., 2011). Large dust particles fall out of the plume early in the dust cycle, leaving clay and silt particles between 0.1 and 20 micrometers in diameter (Adebiyi

& Kok, 2020). Mineral dust in the atmosphere affects the climate indirectly or directly (Fig. 2). The direct effects of mineral dust include scattering and absorbing solar and terrestrial radiation (Albani & Mahowald, 2019). These direct effects can cause the atmosphere to cool (scattering) or warm (absorption). Indirect effects include impacts to cloud albedo and lifetime (Albani & Mahowald, 2019). Dust particles can aid cloud nucleation by acting as cloud nuclei in low cloud condensation nuclei environments (Albani & Mahowald, 2019; Shao et al., 2011). Nucleation efficiency depends on the size and density of the particles; abundant small nuclei prevent precipitation processes because the particles experience many collisions but cannot coalesce (Mahowald & Kiehl, 2003). Aerosols are removed from the atmosphere through dry or wet deposition (Albani & Mahowald, 2019; Shao et al., 2011). Dry deposition occurs when the particle collides with the surface as the result of wind and gravity. On the other hand, wet deposition occurs if the particles are nuclei and fall to the surface as precipitation.

This work did not intend to address the effects of dust and surface interactions through the analysis due to the time scales necessary to study them. Still, dust deposits impact the long-term climate and should be acknowledged because the study spans multiple 5-year periods within the century. For example, dust minerals deposited in oceans contribute to the ocean-atmosphere carbon exchange and excess deposition of iron minerals in the sea can slow the exchange, increasing atmospheric carbon (Shao et al.,2011). Dust deposition onto ice and snow increases the surface albedo, and melting can occur, leading to the release of carbon into the atmosphere (Shao et al., 2011).

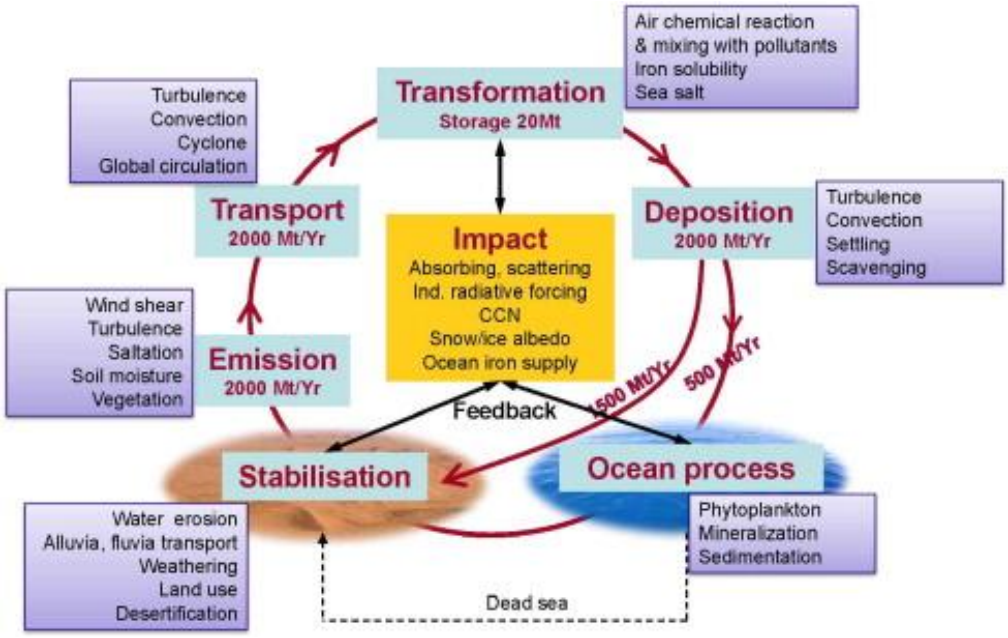

Figure 2. The main processes that are influenced by the dust cycle (Shao et al., 2011).

2.2.1 Dust Impacts in the Luquillo Mountains

As part of long-term ecological monitoring of the Luquillo Mountains, cloud and rain water samples were collected between 1984 and 2007 to determine the seasonal chemical make up at three sites (Gioda et al., 2013). Analysis of these data suggested that calcium ions from dust made up 75 to 90% of the sample concentrations. These concentrations were the highest during the summer, and the water pH was higher than in other seasons. All samples also consisted of iron, aluminum, and silicon, elements typically found in Saharan soils (Gioda et al., 2013). These results indicate that Saharan dust particles were likely present in and below the convective boundary during these rain events. A comparison of the dusty period from 1980–1989 and the non-dusty period from 1955–1964 suggests that regional precipitation changes from changes in dust are about the same magnitude as those from greenhouse gases (Mahowald et al., 2010). This

means that the dust could affect precipitation to the same degree as anthropogenic climate change.

2.2.2. Dust Impacts and the Saharan Air Layer

The Saharan Air Layer (SAL) is a dust laden, warm, dry layer that extends from west Africa across the tropical Atlantic Ocean (Dunion, 2011). The SAL can be 3 to 4 km thick and contain 50% less moisture than the typical atmosphere (Dunion, 2011). The layer occupies the trade wind region between 550 and 850 hPa, typically above the marine boundary layer. Features of the SAL that influence the potential for rainfall are the consequence of changes to thermodynamic, radiative, and microphysical processes. The strength of the trade wind inversion, the ocean temperature, lower troposphere stability, and cloud microphysics are all directly impacted by the SAL (Fig. 3). This thesis focused on the effects of the SAL due to a strengthening trade wind inversion, but implications on the ocean and clouds may have indirectly appeared in the results. For example, the warm SAL air has been shown to affect the SST and latent heat flux over the Atlantic Ocean (Jordan et al., 2018; Strong et al., 2015; Chen et al., 2020). Though these effects are mostly directly beneath the dust plume, this relationship could affect the region of preferred rainfall formation (Jordan et al., 2018; Strong et al., 2015; Chen et al., 2020). For this reason, it is important to acknowledge the multiple ways the SAL can impact rainfall and consider their roles.

The temperature inversion created by the SAL increases atmospheric stability and limits updraft and moisture availability for daily convection and tropical cyclone development (Prospero & Mayol-Bracero, 2013; Dunion, 2011). Rising air cools adiabatically until reaching the warmer and less dense SAL air, where the vertical extent of a cloud is capped (Fig. 3; Powell, 1990). Additionally, when the dry SAL is present in the updraft region of a cloud, the air

parcels are stabilized through evaporative cooling, limiting further cloud development (Powell, 1990). As previously mentioned, nucleation is dependent on particle density. The particles in the layer also aid in inhibiting rainfall by decreasing nucleation efficiency in the collision process. This contributes to the layer's ability to absorb incoming radiation, thus strengthening the inversion and preventing nucleation. Fig. 3 shows the increase in cloud size as the dust intensity becomes more diluted.

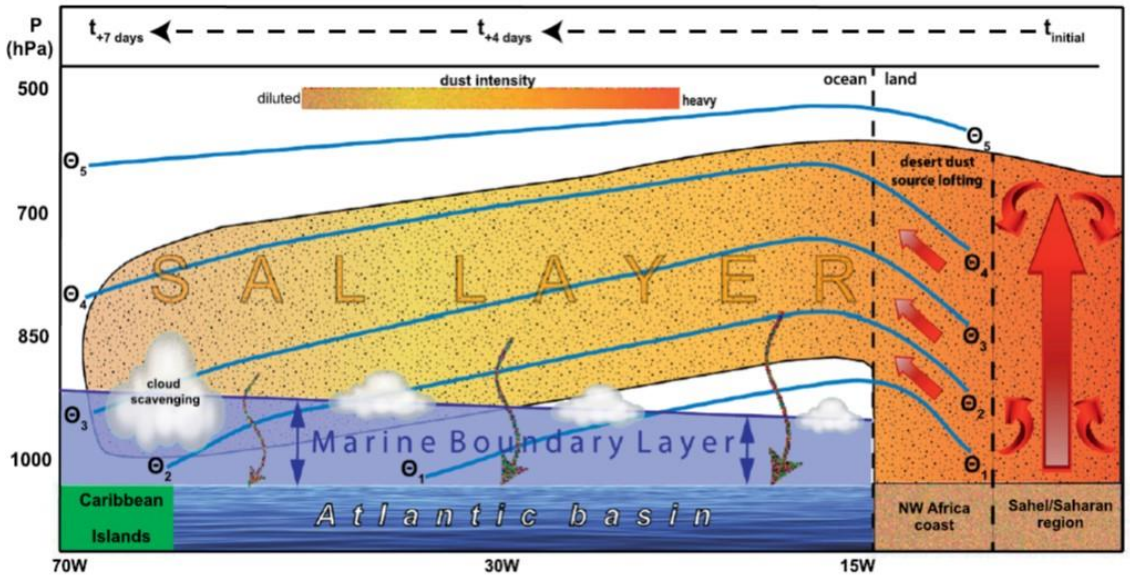

Figure 3. Vertical profile of SAL air mass transported westward from its Saharan source region. Large dust particles are depicted in a red shade, while finer particles are in yellow. The vertical brown arrows represent deposition. Contours of potential temperature are in blue, and the marine boundary layer is shown sloping from east to west from Kuciauskas et al. (2018).

2.3. Tropical North Atlantic Dust Transport

Mahowald et al. (2010) investigated 20th Century causes of dust variability. They found that climate drying contributes to the increase in desert dust during the period, along with other factors, including carbon dioxide fertilization and human land use change (Mahowald et al., 2010). The 2021 IPCC Report supports continued drying in West Africa through the 21st Century (Arias et al., 2021). The dust emission for this region increased from the 1950s to the 1980s and is the most significant contributor to perturbations in the dust emissions globally (Mahowald et al., 2010; Albani & Mahowald, 2019). Future dust emissions cannot be accurately predicted for several reasons: the historical record is still being developed (Albani & Mahowald, 2019; Williams et al., 2016), the spatio-temporal trends are difficult to track (Schepanski et al., 2017), and dust is dependent on several natural and anthropogenic factors such as wind speed and land use that are not well characterized or represented in Global Climate Models (GCMs).

The spatio-temporal patterns for Atlantic dust are influenced by NAO and ENSO from December to February (Doherty et al., 2008). Meteorological observations suggest that dust accumulates in the surface layer near the eastern tropical Atlantic during these months due to advection from the land surface, but as upper and lower-level wind patterns shift with the seasons, transport across the Atlantic becomes more efficient (Chiapello et al., 1995; Barkan et al., 2003). This leads to the transport of dust over the western Atlantic peaking in June and July.

Though the dust aerosol load has a known seasonal trend, the mineral load and timing vary (Fig. 4; Doherty et al., 2008; Prospero & Mayol-Bracero, 2013). Compared to 1979–1983, the 1988–1992 dust season began earlier and transported a larger quantity of dust into the Caribbean (Fig. 4). Additionally, Doherty et al. (2008) showed that the dust plume had shifted

further north in March–May during 1988–1992 compared to 1979–1983. These changes are consistent with anticipated earlier and larger dust intrusions into the Caribbean.

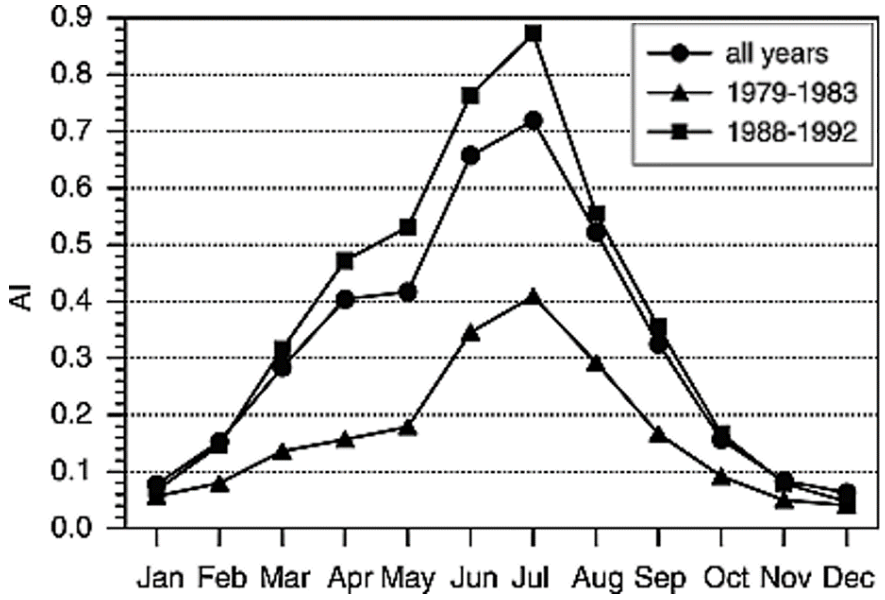

Figure 4. Doherty et al. (2008) TOMS AI analysis revealed a seasonal dust trend, with a maximum in the summer months of Jun–Aug and a minimum in the winter months, Dec–Feb. Monthly mean AI values were spatially averaged over the region 59º–70º W, 10º–20º N, and temporally averaged over different periods.

Past dust outbreaks have shown that transport from the Sahara across the tropical Atlantic typically takes about one week (Barkan et al., 2003; Gioda et al., 2013; Reid et al., 2002). The Puerto Rico Dust Experiment (PRIDE) in July 2000 over the Caribbean islands and waters of Puerto Rico, St. Croix, and St. Thomas was consistent with monthly and seasonal evidence of variability in the mineral load. During the experiment, five dust events that each took

approximately 5–6 days to transit the Atlantic were recorded (Reid et al., 2002). PRIDE also found that the vertical dust column was highly variable between events. As a result of the dust events, the column could extend from the surface to an altitude of 5.23 km (Reid et al., 2002). When the dry column reaches the tropopause during the MSD, the region may remain dry until a tropical wave provides sufficient moisture to overcome the SAL (Reid et al., 2002).

2.4 Drought Onset, Measures, and Implications

Dryness or drought is a complex phenomenon; as a result, the onset, conclusion, and impacts can be relative to the location and application (Seneviratne et al., 2012). Drought events occur when a deficit in precipitation causes drier-than-normal conditions and water problems, such as declines in streamflow (USGS, n.d.). Warmer air can also trigger drought conditions by increasing atmospheric moisture demand. In response to the atmospheric demand, evaporation increases, and surface drying is induced until the demand is met (Ault, 2020). Long periods of meteorological drought can lead to agricultural, hydrological, and socio-economical droughts. A simple model of the phenomena can be described mathematically by a water budget:

$$P - E = \frac{dS}{dt} + R_O + G_w \quad (1)$$

A deficit in precipitation (P) or increased evapotranspiration demand (E) influences soil moisture storage ($\frac{dS}{dt}$), runoff (R_O), and groundwater flow (G_w) (Ault, 2020).

Meteorological drought and its scale can be measured by indicators like precipitation and soil moisture anomalies, and drought indices. Indices typically either describe precipitation independently or along with evapotranspiration and water storage. Drought assessments in the Caribbean are difficult due to limited availability of data (Herrera & Ault, 2017). The Global Historical Climatology Network has fewer than 50 stations on Puerto Rico, with significant

spatial gaps. These gaps make it difficult to assess how drought impacts the island, depending on topography. Additionally, most existing gridded drought products are at spatial scales too coarse to resolve local effects (Herrera & Ault, 2017).

GCMs, such as the Coupled Model Intercomparison Phase 5 (CMIP5), project that the impact of warmer temperatures is expected to increase drought risk globally due to increased evaporative demand (Dai, 2013; Dai & Zhao, 2017; van der Schrier et al., 2013). Regional assessment of model results show that future precipitation declines are expected to be the greatest in the tropics and subtropics. CMIP 6 supports an increase in agricultural and ecological drought, but the change in hydrologic drought is uncertain (Gutiérrez et al., 2021). The Caribbean region could experience diminished rainfall totals up to 50% of the average (Hartmann, 2013; Zhao & Dai, 2015; Ramseyer et al., 2019). Caribbean-wide, June, July, and August, the MSD months, are expected to have the most significant decrease in precipitation (Gutiérrez et al., 2021).

For the Luquillo Mountains, including the El Yunque National Forest, predictions for declines in precipitation implicate increasing dry life zones at the expense of wet life zones (Zinnert et al., 2021). Van Beusekom et al. (2017) showed that Luquillo may be more vulnerable to wet-season drought, with cloud levels approximately equal in the dry and wet seasons. Increased atmospheric demand near tropical mountain cloud forests alters direct and indirect moisture availability by perturbing the cloud height and elevational temperature (Foster, 2001; Martin et al., 2011; Zinnert et al., 2021). The average altitudinal range of plant, tree, and animal species is heavily affected by climate changes, posing a high risk of loss in the future (Laurance et al., 2011; Van Beusekom et al., 2015; Zinnert et al., 2021).

Analysis of the 2015 drought suggests that regions of Luquillo are resistant and resilient to short-term droughts. Vegetation greenness and canopy moisture levels returned to normal within a year, and plant mortality was consistent with non-drought years (Schwartz et al., 2019). The resistance and resilience of the forest moisture have not been analyzed over more extended periods of drought or a dryer climate (Schwartz et al., 2019). For locations like Puerto Rico that need more localized studies but lack available data, downscaled GCM output offers a way to explore drought and analyze possible long-term effects. The future climate knowledge learned through downscaled GCMs can also assist in the management of Luquillo to encourage greater resistance and resilience.

CHAPTER 3

Research Design

3.1 Research Objectives

Though the Sahara has long been known as a dust source and the Caribbean a dust sink, the variability in the timing and amount of Saharan dust emitted and transported continues to plague drought prediction (Miller & Ramseyer, 2020; Prospero & Mayol-Bracero, 2013). GCMs are a tool that allows for future dust and precipitation scenarios to be generated and analyzed. GCMs present the most effective way to communicate climate impacts due to their coupled ability, but the spatial scales represented often are not fine enough for regional or local assessments. Dynamical downscaling is one technique used to refine GCM output. This technique derives the effects of large-scale climate processes for a region or location of interest from high-resolution regional simulations.

In general, this research builds upon current work investigating the strength and frequency of the trade wind inversion and modeling the convective thermodynamic structure of the atmosphere during SAL outbreaks. Past modeling work has statistically downscaled CMIP5 Representative Concentration Pathway (RCP) 8.5 predictions for ERS rainfall and reproduced the thermodynamic environment that contributed to the intensity of the 2015 drought, but it remains unknown if early rainfall season intrusions like the April 2015 event will continue to play a critical role in drought onset (Ramseyer et al., 2019; Miller et al., 2021). I fill this knowledge gap by exploring the potential impact of global sea surface warming on the length of the dust intrusion period using the RCP 8.5 scenario to simulate the predicted warming. RCP 8.5

depicts the climate under a worse-case warming scenario, with a radiative forcing of 8.5 Wm^{-2}. Because climate stability is critical for the LUQ, I also investigated how atmospheric moisture is influenced by the length of the intrusion period by analyzing hydrometeorological variables.

3.2 The Weather Research and Forecasting Model

The Weather Research and Forecasting Model (WRF) is a mesoscale numerical weather prediction model with operational weather forecasting and atmosphere research applications. WRF is an atmosphere model that can be run with enhanced chemistry settings and additional parameterizations, such as land and radiation. WRF-chemistry can calculate and output emission and gas element features. WRF-chemistry 3.8.0 was compiled, and simulations for three five-year periods were conducted to model dust emission and transport from the Sahara and the Middle East across the Atlantic and into the Caribbean basin. The periods consisted of the historical period (H) 2013–2018, mid-century (MC) 2045–2049, and end-century (EC) 2085–2089. In total, six simulations were performed.

Miller et al. (2021) conducted nine simulations to determine the dust configuration that best modeled the March 1– May 31, 2015, dust outbreak. These simulations and those undertaken for this study were run on the same 64 km resolution domain (Fig. 5). Though WRF has several options for dust emissions schemes, two were tested by Miller et al. (2021): (1) Georgia Tech/Goddard Global Ozone Chemistry Aerosol Radiation and Transport (GOCART) and (2) GOCART with Air Force Weather Agency Modifications (GOCART-AFWA). The GOCART scheme has been widely used in WRF-Chem studies since included in the model version 3.2, but in 2011 the Air Force Weather Agency identified certain environmental conditions could cause the GOCART scheme to be invalid within WRF (LeGrand et al., 2019).

The GOCART-AFWA scheme was developed to address issues with GOCART under eroding of soil particles. The dust emissions scheme, GOCART-AFWA, best represented WRF-Chem AOD and Gálvez-Davison Index (GDI) against the same products from ERA5 and NASA Terra Moderate Resolution Imaging Spectroradiometer (MODIS) and NASA's Aerosol Robotic Network (AERONET) during the period.

Miller et al. (2021) also tested the dust emission sensitivity of the model with various tuning parameters. Tuning parameters modify the onset and the magnitude of dust emission but are usually best for regional models (Flaounas et al., 2017). These simulations were conducted to show the source to sink dust transport from the Sahara to the Caribbean, so the default of 1.0 showed the most reasonable results. Simulations referred to as 'dust on' simulations all employ the GOCART-AFWA (i.e., dust_opt = 3) aerosol scheme. The 'dust off' simulations turned off all atmospheric chemistry (i.e., chem_opt = 0).

Historical simulations used boundary conditions from the ERA5 reanalysis dataset. Alternatively, MC and EC simulations utilized the Community Climate System Model (CCSM) CMIP5 RCP8.5 dataset. Direct radiative effects were turned on, allowing dust to modify the atmospheric layer thermodynamically. This parameterization selection allows dust emission levels to alter the dust load and structure of the SAL. Other parameterization schemes and domain configurations can be found in Table 1.

Table 1. Parameterization and Domain Settings for the WRF-Chem Simulations

Setting	**Option**
Grid Spacing	64 km, 16 km
E-W grid size	252, 73
N-S grid size	68, 53
Vertical levels	40 (historical), 38 (future)
Boundary layer	YSU scheme
Land Surface	Noah land-surface model
Radiation	RRTMG
Cumulus	New Tiedke scheme
Microphysics	WSM6
Chemistry	GOCART simple aerosol
Dust	GOCART-AFWA

Dynamically downscaling the coarse resolution GCM output provided greater detail of how changes affect the Luquillo Mountains with their steep elevation, precipitation, and ecological gradients. Both 64- and 16-km resolution model simulations were conducted and analyzed, with the 16 km being the result of dynamically downscaling the coarser model runs (Fig. 5). One-way nests centered on Puerto Rico were run, and output from the coarse resolution domain was used to derive AOD. The 16 km grid simulation output provided air temperature, precipitation, and relative humidity. The temporal length, relatively high spatial resolution, and

interactive chemistry make the 16 km simulations computationally expensive, so these outputs were analyzed for three-year windows from 2014–2016 (H), 2045–2047 (MC), and 2085–2087 (EC).

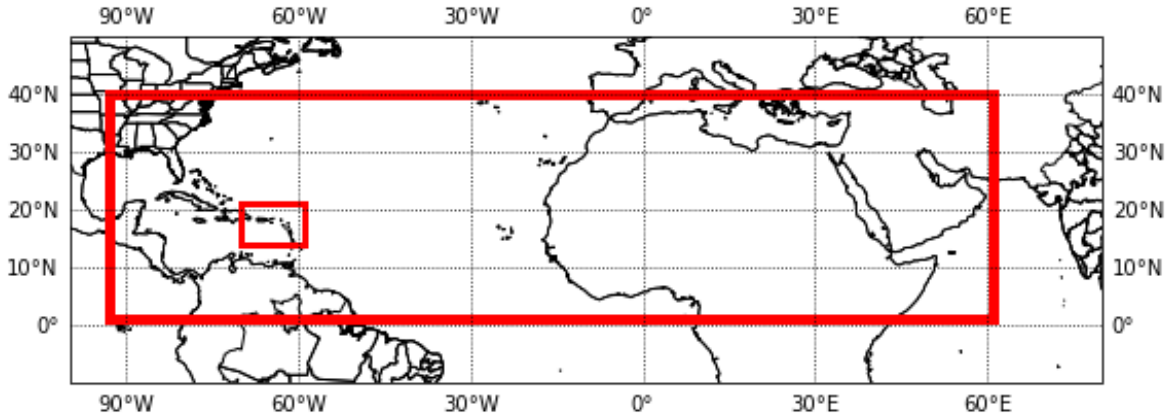

Figure 5. 64 and 16 km domains used in WRF simulations. 16 km simulations were dynamically downscaled from the 64 km.

CHAPTER 4

Methods

4.1. Aerosol Optical Depth (AOD)

Recent work suggests that Atlantic SSTs influence dust transport and not vice versa (Wong et al., 2008; Chen et al., 2020). Wong et al. (2006) showed that an 850-hPa warm temperature anomaly is related to the direction of dust transport across the Atlantic. Further representing SAL cross-Atlantic transport and supporting a link to Atlantic SST variability, Wong et al. (2008) found that higher SSTs indirectly shift the transport path. Increases in tropical Atlantic SSTs result from anthropogenic climate forcing and were modeled in the future boundary conditions. These conditions were assimilated into the WRF-Chem simulations.

Typical measurements of AOD measure the concentration of aerosols in a column of air by the amount of irradiance that reaches the earth's surface. The methods for WRF use the vertical thickness and the amount of light absorbed at 550nm. AOD is an index from 0 to 1. Values less than 0.1 reflect clear sky conditions. In contrast, values closer to 1 indicate a hazy sky and the presence of many aerosols. WRF 550nm extinction coefficient, perturbation geopotential, and base-state geopotential output were used to calculate AOD (equation 2). The base-state geopotential is constant and was set during simulation initialization based on the location geography. Perturbation geopotential starts at zero and varied over the simulation period. The sum of the base-state geopotential and perturbation potential in units of m/s^2 are described as dz in equation 2.

$$AOD = \frac{550nm\ extinct\ coef}{1000} * dz \quad (2)$$

AOD data from WRF-chem were compared to Terra- MODIS satellite AOD for 2014–2018 at monthly scales to assess the validity of the WRF-Chem output (Platnick et al., 2015). Magnitude differences were quantified using percent difference (equation 3).

$$\text{Percent Difference} = |\text{WRF\_AOD} - \text{MODISAOD}| / ((\text{WRF\_AOD} + \text{MODISAOD})/2) \times 100\% \quad (3)$$

The monthly average AOD for Puerto Rico during each period was analyzed to assess changes in the dust season. Monthly average pressure heights, wind speed, and direction provide insight into the tropical North Atlantic (TNA) dust transport system. This information assisted in assessing if the effects on hydrometeorology can be attributed to the dust-laden SAL.

4.2 Hydrometeorology

Water resources and availability are broad concepts, encompassing the demand, supply, and access to water. The complex feedback between dust, temperature, and clouds increases uncertainty about future water availability. Future perturbations to water resources in Luquillo could have detrimental impacts on the forest structure (Zinnert et al., 2021). As previously discussed, dust can impact atmospheric processes in multiple ways. Suspended dust particles can act to block solar radiation, causing lower temperatures below the dust layer. On the other hand, dust can be packed into the SAL and contribute to atmospheric warming. The warming increases stability in the atmosphere and limits convective rainfall development.

Cloud location and micro-physics are also influenced by dust presence in the terrestrial boundary. Evidence during SAL intrusions shows a southerly displacement of clouds (Wong et al., 2006; Wong et al., 2008) and limited convective precipitation (Mote et al., 2017; Miller et al.,

2020). It is also important to note that the highest elevations of the Luquillo Mountains are almost always within the cloud deck. This supplies the surface soils and canopy with direct moisture, even when rainfall is not occurring. Without these clouds, the associated temperature change induces evapotranspiration rate change.

WRF output includes rainfall, but because dust can both increase and decrease rainfall, a convective forecasting index is included in the analysis to better determine if changes are attributed to the SAL's effects on the thermodynamic environment or other climate drivers. Additionally, the index used in this analysis was calculated from model output, making it almost independent from the convective parameterizations used in the simulations (WRF Single-Moment 6-Class Scheme (WSM6), New Tiedke scheme) and providing a more realistic representation of where it will rain. The convective index employed in this work was the Gálvez-Davison Index (GDI). Developed to forecast tropical convection, GDI has previously been used to assess the atmosphere's thermodynamic structure for hydrometeorological analyses (Gálvez & Davison, 2016; Miller & Ramseyer, 2020; Miller et al., 2017). GDI values range from -20 or less to +45 or greater (Table 2). Positive values indicate atmospheric instability; warm and moist air is below cooler and drier air. Negative values relate to a stable atmosphere, where cool and dry air is at the surface. The more positive a GDI index value is, the greater the chance for scattered or widespread thunderstorms. The overall GDI index value is derived from potential temperature, temperature modulations at 500 hPa, and the temperature difference between 950 and 700 hPa.

Table 2. Critical GDI Values and Convention Type

GDI	Expected convective regime
>+45	Scattered to widespread thunderstorms
+35 to +45	Scattered thunderstorms and/or widespread shallow convection
+25 to +35	Scattered shallow convection and isolated to scattered thunderstorms
+15 to +25	Isolated to scattered shallow convection and a few isolated thunderstorms
+5 to +15	Isolated to scattered shallow convection; any thunderstorm brief and isolated
-20 to +5	Isolated to scattered shallow convection; strong subsidence inversion likely
<-20	Fair conditions, any convection should be shallow, isolated, and produce light rain

To inclusively account for atmospheric moisture demand impacts through meteorological, hydrological, and ecological drought, WRF output for temperature and relative humidity were used to calculate vapor pressure deficit (VPD). VPD is a meteorological term to describe the difference between the amount of moisture in the air, the actual vapor pressure, and the maximum amount of moisture in the air at a given temperature, the saturation vapor pressure (equation 4).

$$VPD = e_s(T_a) - e_a \quad (4)$$

Where e_s is saturation vapor pressure, e_a is the actual vapor pressure, and T_a is the air temperature. VPD is recorded as pressure in kilopascals (kPa) units, and saturation decreases the

further the difference is from 0 kPa. VPD increases have been related to land evapotranspiration limitations and photosynthesis declines (Barkhordarian et al., 2019; Yuan et al., 2019). These relationships make it a drought indicator and a unique meteorological observation for examining tropical forest moisture and plant function.

To address research question 2, rainfall, GDI, and VPD variables calculated from 'dust on' and 'dust off' simulations as seasonal averages were compared through various analyses. The 'dust on' and 'dust off' values were first tested for normality with Shapiro-Wilks tests in R. After normality was determined, either a paired t-test or a Wilcox statistical test was used to determine the effect of dust on the variables. The test selected to compare the data was dependent on the data normality. In addition to determining the effect of dust during a specific period, the change in moisture for both simulations was also analyzed. Percent change calculations were performed in R to assess the change from historical to future periods and between the two periods (equation 5). The 'dust on' and 'dust off' simulations were analyzed separately for this portion of the analysis.

$$\text{Percent Change} = \frac{|\text{future value} - \text{previous value}|}{\text{previous value}} * 100\% \quad (5)$$

4.2.1 Precipitation Bias Correction

The WRF model itself has a bias in all output because it is a numerical model. The GDI is included in this analysis to assess the thermodynamic properties that effect rainfall potential, but the actual rainfall values and locations are useful in quantifying the possibility of drought. Before precipitation data can be analyzed, a Model Output Statistics method of precipitation bias correction was employed. The method first derives a bias-corrected precipitation factor (BC_p) from the mean observed precipitation ($\overline{P_O}$) divided by the control model precipitation (P_{MC};

equation 6). The final precipitation (P_f) is then derived from the future model precipitation magnitude (P_{MF}) and the bias corrected factor (equations 7).

$$BC_p = \frac{\overline{P_O}}{P_{MC}} \quad (6)$$

$$P_f = P_{MF} * BC_p \quad (7)$$

The Model Output Statistics procedures were beneficial because it reduced the model divergence from the observations to the smallest degree possible. For this analysis, NASA Integrated Multi-satellitE Retrievals for GPM (IMERG) precipitation data served as the observations (O), and the historical dust on output was the mean control model (MC; Huffman et al., 2019). The IMERG data were scaled from their original 11 km grid to the WRF 16 km grid, so the corrected rainfall contained a greater degree of accuracy. Rainfall from the historical 'dust off' and all future simulations were corrected as the future model (MF). The use of a change factor statistics approach allowed the change between periods to be conserved as the values were corrected.

CHAPTER 5

Results

This section presents an analysis of 21st-Century AOD in relation to predictions of atmospheric pressure systems. AOD assessed as monthly, early rainfall season, and dust season averages allowed multiple analyses of the period's dust climatology. The 2015 dust and drought events suggest the model representations of early-season dust outbreaks and the resultant moisture responses. Rainfall, convection, and vapor pressure deficit were analyzed over historical (2014–2016), mid-century (2045–2047), and end-century (2085–2087) periods. Each moisture environment variable served a purpose with a connection to the SAL and drought. Convection describes the SAL interaction in cloud and storm development, rainfall details the cloud and rain processes, and VPD describes the atmospheric demand.

5.1 WRF AOD Error

Model AOD performance was considered to assess the validity of the magnitude and timing of Puerto Rico dust intrusions. Model performance was determined through percent difference calculations from the MODIS satellites AOD product. All AOD analysis uses the coarse resolution output, which allowed the full transport path to be analyzed. The model performance analysis is focused on Puerto Rico's historical AOD and not the entirety of domain 1 because the spatial analysis was bounded by Puerto Rico's extent between 17.84°N to 18.57°N and 65.21°W to 67.96°W. Additionally, transport timing and Puerto Rico's dust magnitudes were more critical to this analysis than emission magnitudes over Saharan Africa.

Previous work that established the best model setup resulted in WRF-chem AOD estimates greater than Terra MODIS and AERONET. Similarly, the simulations conducted for this work resulted in overestimated monthly dust magnitudes (Fig. 6). Nonetheless, the seasonality of dust was captured. The AOD magnitude error increased as the dust season progressed, with August displaying the greatest percent errors. The additional dust in the model could be due to Terra MODIS being a composite of 24-hour AOD, while WRF AOD is an average of 4 instantaneous times per day. If one time stamp is over simulated, the overall daily WRF AOD would be too high. Additionally, MODIS data had to be interpolated from 1° resolution (approximately 111 km) to 64 km to be compared to the WRF output. Since the observed dataset had less spatial accuracy than the model data, there are spatial differences that may be simulated by the model, but not reflected in observations.

For Puerto Rico, during ERS months, the model overpredicted up to 10% of the AOD. The lower error during the ERS, compared to the MSD, could correspond to the influence of clouds (Fig. 6). AOD days with cloud cover equal to or greater than 0.1 were excluded from the model analysis to eliminate cloud contamination in the height perturbation output used in the dz term of the AOD calculation. The exclusion of these cloudy days could also drive the seasonality differences in WRF's ability to predict magnitudes. The model performed better over larger land masses in the eastern Caribbean, like Puerto Rico. This could be due to the model responding to land and ocean radiative differences.

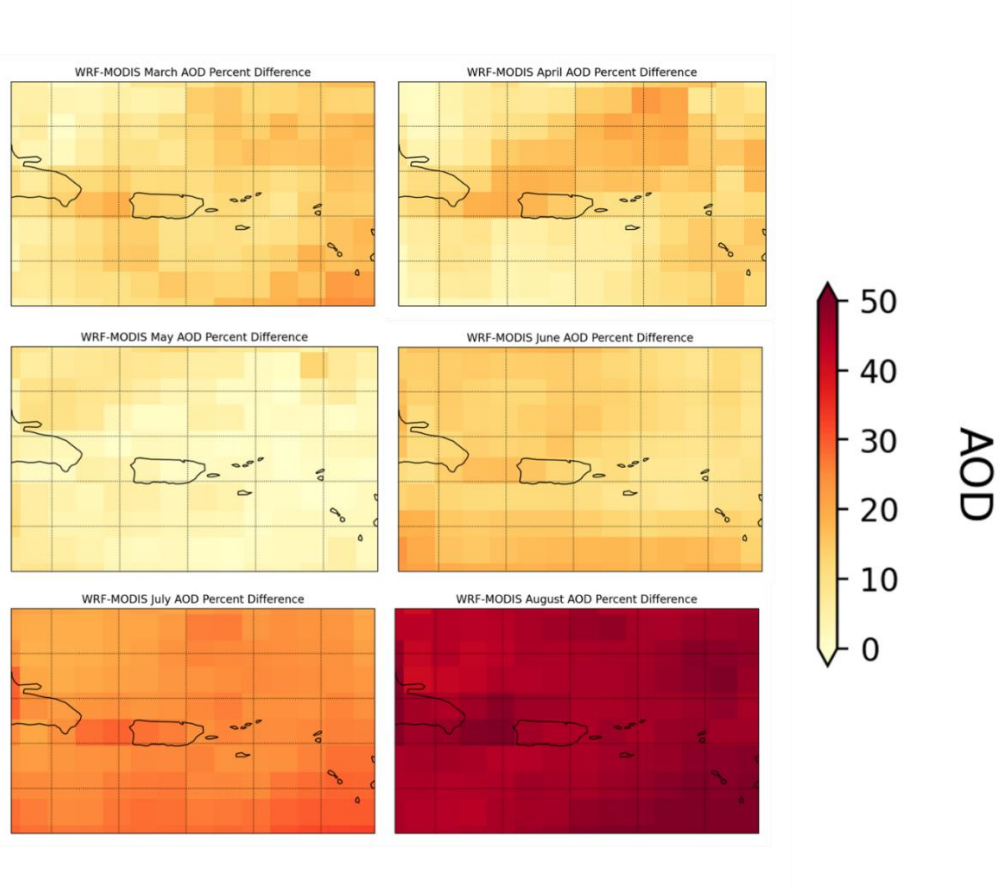

Figure 6. Historical mean monthly AOD percent difference from Terra MODIS mean-monthly AOD.

5.2 Synoptic Environment

5.2.1 2015 Case

Considering that the historical simulations were the baseline in this analysis, the 2015 anomalous dust outbreak in the ERS was analyzed to ensure that the model represented known events. As previously discussed, the NAO plays a significant role in dust transport across the TNA and drought in the Caribbean. During the 2015 drought, a positive NAO strengthened both the NASH and Caribbean Low-Level Jet (CLLJ), leading to an increase in trade wind windspeeds beginning in March 2015 and continuing until February 2016 (Herrera et al., 2020;

Mote et al., 2017). The WRF model characterized the ERS of 2015 with lower heights (pressure) and faster wind speeds compared to the entire historical period (Fig. 7).

With an expanding NASH during this period, heights are expected to be near normal or increased. Though the heights were lower than the period average, the expanded NASH is slightly north of Northern Africa, and isoheights are closely grouped, indicating quickly changing heights in the north Atlantic, both features associated with a positive NAO (Fig. 7; Appendix A). The change in height with latitude results in higher surface wind speeds from the northeast during the season. This increase in wind speed is correlated with anomalous trade winds that advected dust across the Atlantic during April. ERS temperature at the surface and 850-hPa also indicated lower or near normal temperatures for Puerto Rico and the eastern Caribbean (Fig. 7). Lower temperatures in 2015 may indicate that the surface air was cooler and drier than normal, resulting in greater stability, and less convection and rainfall than typical for the season.

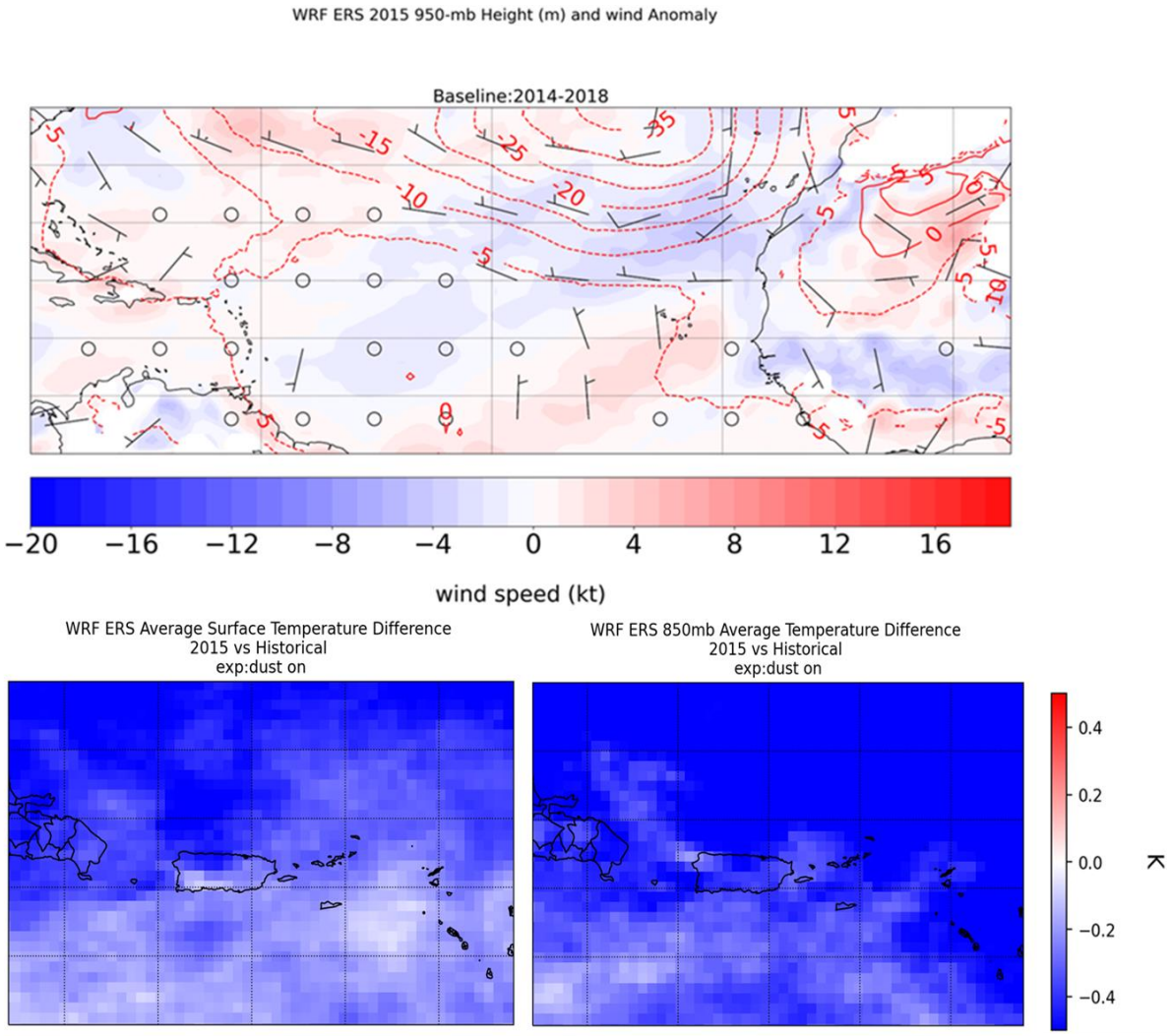

Figure 7. 2015 early rainfall season average height, wind, and temperature anomalies. The baseline period for analysis is the full historical period (2014–2018). Top: surface height and wind speed anomaly; left: surface temperature anomaly; right: 850 hPa temperature anomaly.

Fig. 8 shows the vapor pressure deficit anomaly at 850 hPa for April and June averaged over the ERS of 2015. These figures further indicate that the 2015 season had the greatest influence on the 2014–2016 period. Moisture impacts from the SAL could be evident at the bottom of the layer, typically near the 850 hPa pressure level. April and ERS averages of VPD in

2015 reflect anomalies of a more saturated atmosphere than the historical average in eastern Puerto Rico but less saturated in the western portion of the island (Fig. 8). June anomalies indicated greater moisture over the water bodies near the Caribbean but slight dryness or near-normal conditions over Puerto Rico.

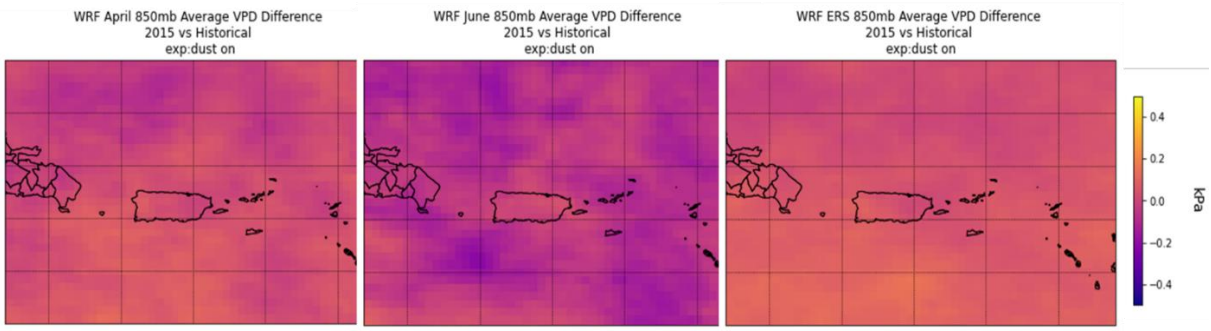

Figure 8. Vapor pressure deficit anomalies for April 2015, June 2015, and over the entire ERS. A baseline of 2014–2017 is used to calculate anomaly.

5.2.2 Model dust and synoptic representations

To further understand the relationship between the model synoptic environment and model dust, the model ability to transport dust in 2015, as well as the conditions during the intrusions, were analyzed. The WRF model over-simulated erosion in the Sahara during all seasons but resolves the transport areas well (Fig. 9). The model better simulated the amount of dust transported than eroded, meaning that near the Caribbean, WRF AOD is similar to MODIS AOD for the respective period. 850-hPa heights and wind speeds in April show established transport paths across the Atlantic, as noted by geostrophic easterly winds (Fig. A1). In April

2015, dust advected off the coast of Africa spanned a larger coastal region in the model simulations than MODIS, but dust was accurately transported across the southern north Atlantic by high pressure centered in the central Atlantic (Fig. A1). The greatest concentration of dust in April mostly moved over the Lesser Antilles and South America.

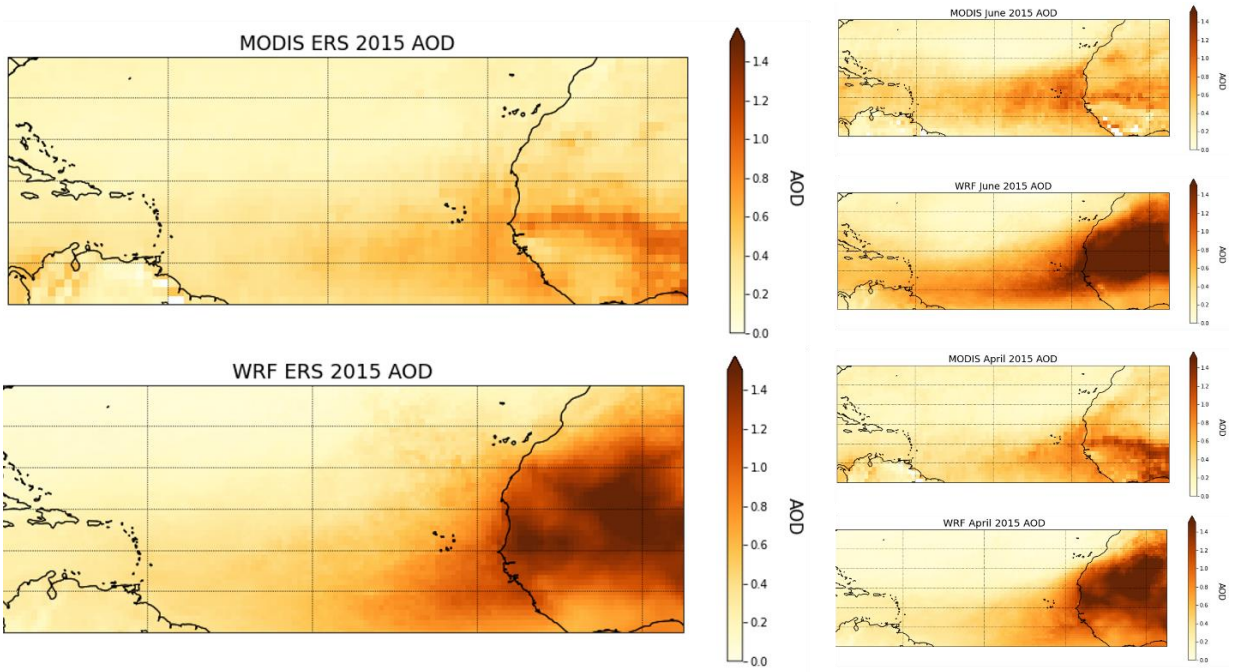

Figure 9. WRF modeled, and MODIS AOD averaged for April, June, and the early rainfall season of 2015.

By June, 850-hPa heights within the transport region increased, as the NASH strength increased. In addition to the strengthening of the high pressure between April and June, the pressure contours expanded to the southwest (Fig. A2). The change in height with latitude led to

increased wind speeds, while the direction of expansion allowed dust flow to reach northern Atlantic regions that include the Caribbean.

Above the SAL region, the 500-hPa heights indicated the development of an upper air trough between April and June in the tropical Atlantic (Fig. A2). The trough, extended from the northeast Atlantic, further identified high pressure near Europe. Trough height and location show cool upper-level air unable to penetrate regions where warmer air associated with the SAL exists. The environment from April to June agrees with a strengthening of the trade wind inversion during the dust season and is spatially consistent warm temperatures below the SAL.
Overall, during the ERS, WRF overpredicted the dust magnitude but the atmospheric environment showed elevated dust levels during appropriate periods in 2015 (Fig. 10). At 850 hPa, the season average wind direction is from the northeast, guided by a weak high-pressure system in the central North Atlantic. Speeds in the transport region were primarily between 12 and 16 knots (6 – 8 m/s), supporting the possibility of wind-assisted dust transport in the mid-troposphere. Winds in the upper troposphere were not zonal and showed rotation in the wind direction across the Atlantic. Though a slight trough is present in the season-averaged height, it is not as evident as in June. The 2015 ERS average wind speed contours at 500-hPa depicted a pattern similar to the April average, suggesting the early season pattern remained for an extended period.

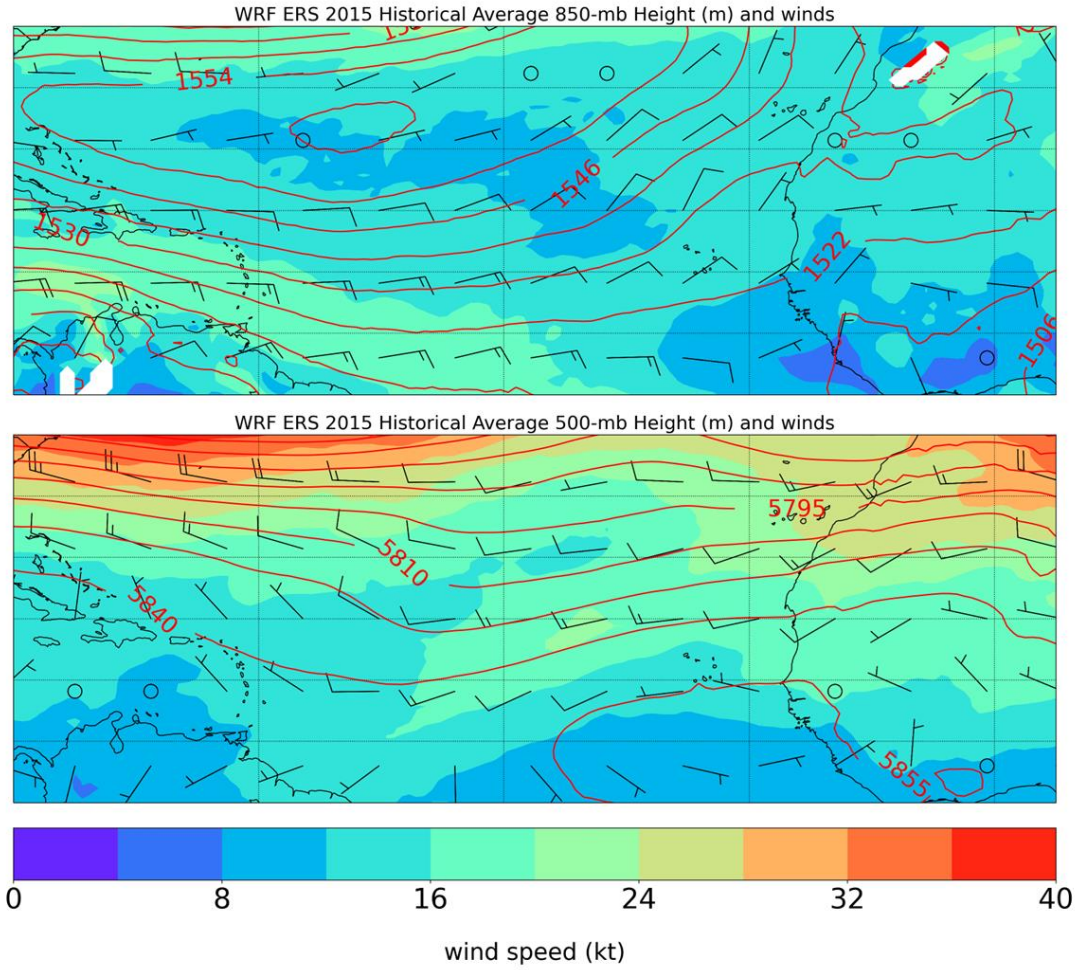

Figure 10. 2015 ERS averaged 500 and 850 hPa heights, wind speed, and wind direction.

5.3 Annual Dust Season

Considering the influence of a warming ocean on the atmosphere, pressure level heights are expected to increase in the future. Between the historical period and the mid-century, the annual average ERS 850 hPa pressure in the north Atlantic and Caribbean could rise by 5–10 m (Figs. 11, B11). An additional increase of 8–10 m could be expected between the MC and EC (Fig. B11). Increases in atmospheric height might lead to changes in El Yunque's ecosystem. As the cloud level rises the expected heights may cause the cloud base to rise above the forest

surface. The increase in atmospheric pressure expanded the Atlantic and South America areas impacted by dust in the ERS (Fig. 11). Doherty et al. (2008) support that an extended dust season could result from increased dust emissions and/or changes to the transport path. Though the simulations did not suggest increased emissions during the dust season (March–September), they did show a wider region of the Atlantic transporting dust (Fig. 15).

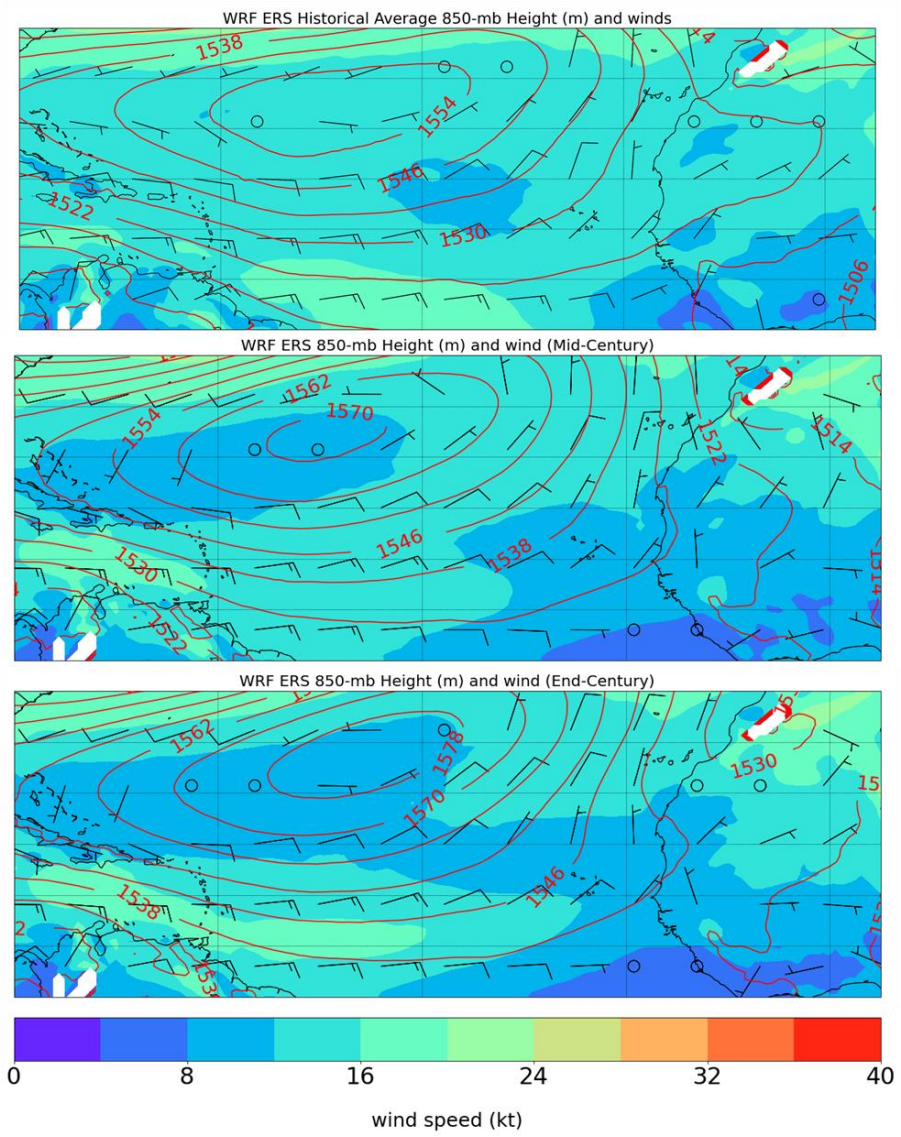

Figure 11. ERS annual average heights, wind speed, and direction at 850 hPa.

The upper atmosphere also responds to surface temperature changes, with height increasing 80–100 m between the H and EC (Figs. B5, B6). This indicates a persistent warm layer below, and likely in the 850 – 500 hPa region, the location of the SAL. Similar to June 2015, the June 500 hPa average heights in the future exhibit a westward extending pressure gradient from the Sahel to the Caribbean (Fig. B2). The upper-level trough in the historical average 500-hPa heights steer higher concentrations of dust into the southern Caribbean, but the emerging future synoptic pattern could develop a more direct path into the Greater Antilles. The movement of the warm air aloft from the Saharan region westward also leads to a more structured wind pattern in the future. The change in wind direction would move warm, dry Saharan air across the Atlantic at faster speeds.

Wind direction and speed changes at 700-hPa are similar to those at 500-hPa. Doherty et al. (2008) found a wind direction shift between the equator and 15°N when comparing the 1989–1993 period to 1979–1983. The change they reported resulted in the ERS plume shifting northward and arriving earlier in the Caribbean. Mid- and end-century ERS average wind direction at 700-hPa shows winds becoming more zonal in the eastern Atlantic, allowing dust to move off the coast during the season. As the dust travels west, during the future period, the direction is either westward or northwestward, both flows that would move dust into the Caribbean (Fig. 12).

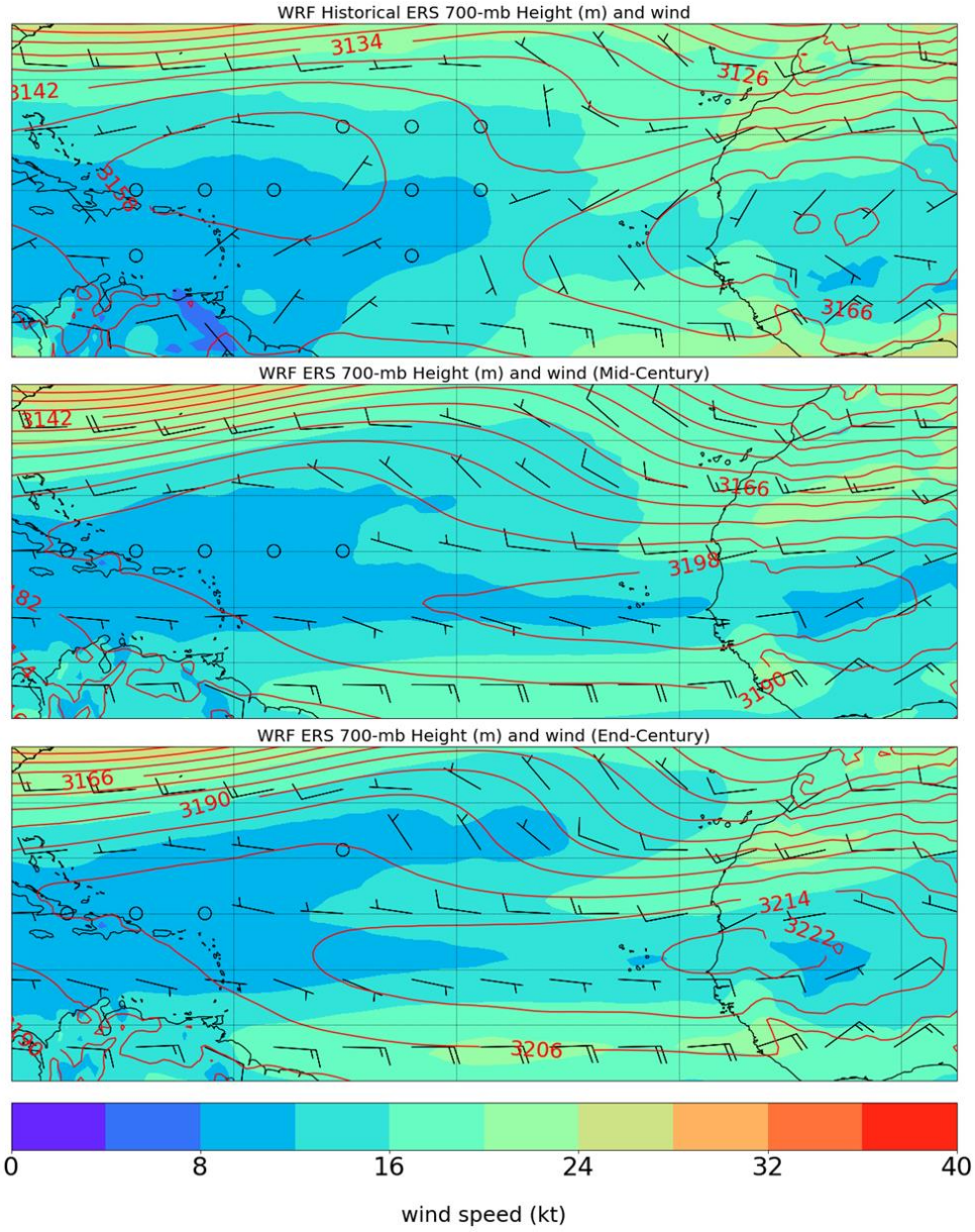

Figure 12. ERS 700 hPa pressure level heights, wind speed and wind direction for the Historical, IC, and EC.

5.4 WRF AOD

5.4.1 Time Series

The historical dust pattern displayed a gradual increase at the start of the season in May, with a steep decline after the peak in September (Fig. 13). The historical AOD monthly mean did increase during the ERS. Most of the increase occurred in April, with March often experiencing the clearest sky conditions of the year. Historically and represented through these simulations, aerosols were more present in the ERS months of April and May. A 0.02 difference in April and May AOD indicates that sky conditions and aerosol volumes were nearly similar.

The location and strength of the NASH strongly influence the direction of the surface winds in the future, supporting continuous dust erosion in the Sahara and subsequent motion into the Caribbean. In the future, aerosol magnitudes are predicted to quickly increase, beginning in April. The July increase of dust aerosols in the MC and yearly variability in ERS months mean AOD contribute to changes in the annual curve (Figs. 13, C2). During the MC, the annual dust season peaked in July, but dust aerosols continued to increase through September. By the EC, AOD indicates an exponential increase in the monthly mean until July, and magnitudes remain the same through September. The July yearly increase in dust suggests a change in the dust season from a one-month peak to three. The annual monthly average AOD did not change between the periods except during the MC when peak season averages are predicted to be the highest of all periods.

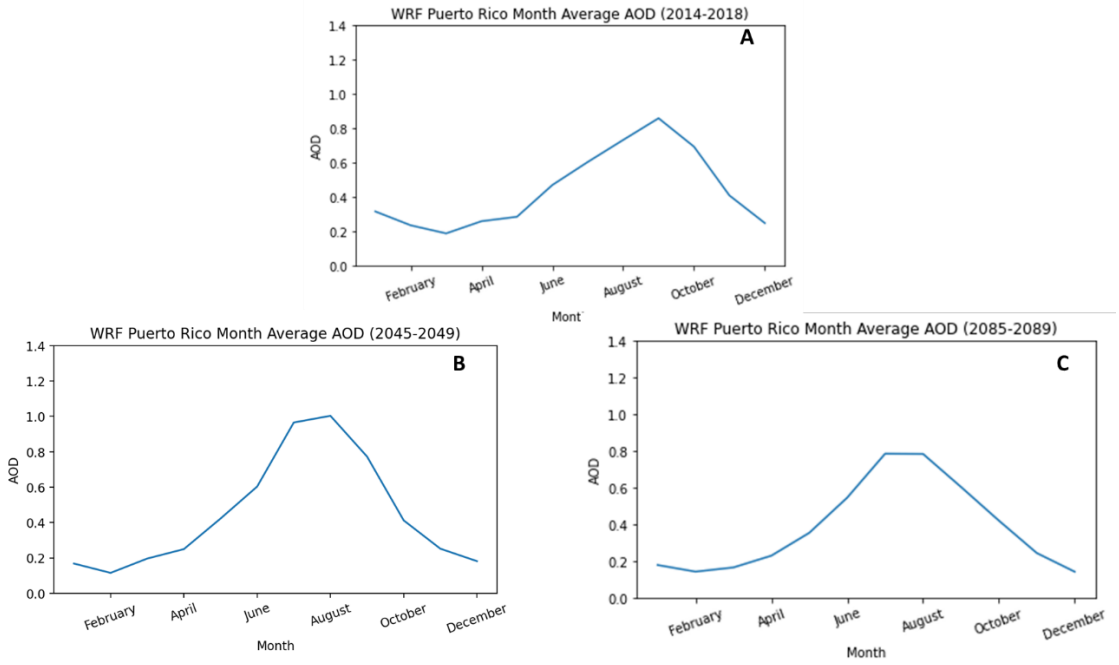

Figure 13. Spatially averaged monthly AOD for Puerto Rico bounded by 17.84°N to 18.57°N and 65.21°W to 67.96°W for (A) the historical period from 2014 to 2018, (B) the mid-century period from 2045 to 2049, and (C) the end-century period from 2085 to 2089.

5.4.2 AOD Spatial Analysis

Spatial analysis of AOD averages during ERS and MSD months agree in magnitude with monthly time series. Although average magnitudes are similar in March and April during all periods, the future periods carry dust into the South American coast instead of the aerosols collecting at the African coast, as the historical records indicate (Figs. 14, D1, D2). On average, less dust is emitted from the Sahara during May of the MC and EC than historically, but higher quantities of dust can reach the Caribbean region earlier due to changes in wind direction and wind speed in the future (Fig. D3). Averaging the monthly means of the ERS months for the

respective periods agrees with a change in dust seasonality. The MC ERS mean has the greatest difference from the historical, where an AOD of 0.2 to 0.6 is recorded for the Lesser Antilles.

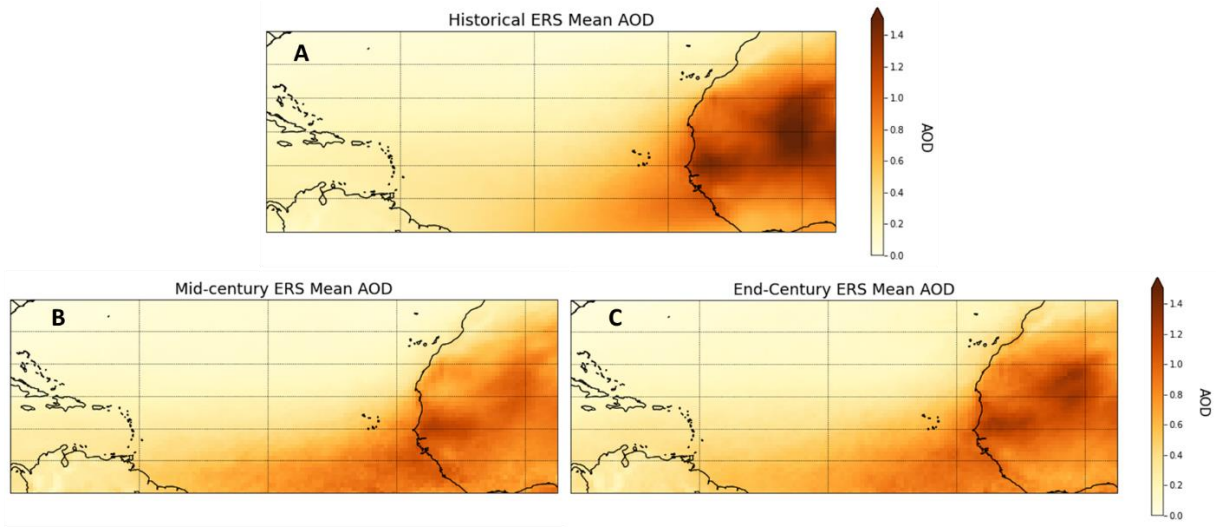

Figure 14. ERS (March–May) averaged AOD. AOD scale ranges from 0 to 1.4, where higher values indicate higher dust magnitudes. (A) historical ERS average from 2014 to 2018; (B) mid-century ERS average from 2045 to 2049; (C) end-century ERS average from 2085 to 2089.

The MSD months of June, July, and August progressively increase AOD during each period (Figs. D4–D6). AOD increases during these months can be attributed to greater erosion in the Sahel and a northward shift in the central transport region. The synoptic maps discussed in Chapter 4 also agree that wind speeds increase in the westward direction during the MSD months. MC AOD is likely the highest because of NASH strength during the MSD months in 2045, 2048, and 2049. Though AOD in the MSD months in 2085 and 2086 is similar to the pattern seen in the MC, the latter 3 years decrease the mean, making the period less dusty (Fig.

C3). These relationships result in a nearly similar dust season AOD average for the MC and EC that are 0.1–0.2 AOD indices different from the historical average (Fig. 15).

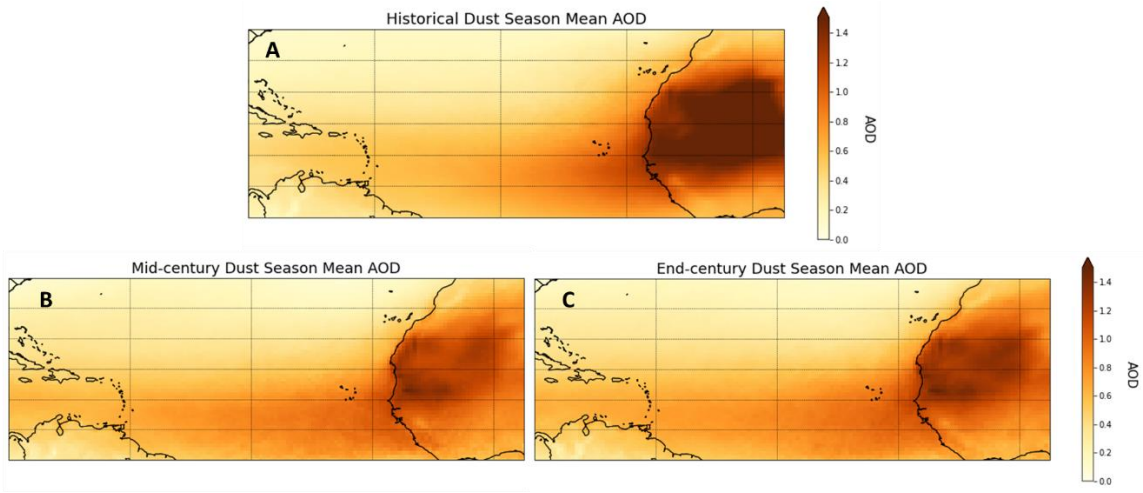

Figure 15. Dust season (March–September) averaged AOD for (A) the historical period from 2014 to 2018, (B) the mid-century from 2045 to 2049, and (C) the end-century from 2085 to 2089.

5.5 Moisture Environment

5.5.1 Precipitation

'Dust on' simulation rainfall from WRF overestimated the annual historical rainfall (Appendix E). Though the 'dust off' annual map better captured the spatial pattern of rainfall observations over the Atlantic and the Caribbean Sea, the dust on map overestimations best reproduced the locations of the greatest and least rainfall. Both simulations and observations agree that rainfall was the highest in the island's western portion. Though the highest annual

precipitation is expected to be near the Luquillo Mountains, the resolution of the simulations limits the ability for this to be reflected and only featured high rainfall in the LUQ region compared to its surrounding.

Annual rainfall does not convey the declines that occur specifically during the early rainfall season. Dust did significantly affect the rain during all periods. The difference in the medians during the mid-century is the least significant of the three periods. The ‘dust on’ and ‘dust off’ similarity in rainfall during the MC highlight that the atmospheric changes because of climate change are similar to the changes induced by dust. Annual and ERS rainfall will decrease island-wide (Fig. 16). Southwest and south-central Puerto Rico remain the area with the greatest precipitation in all periods. By the EC, the LUQ region rainfall decreases by about 1000 mm/yr. A significant amount of this decline is during the ERS, with Luquillo rainfall decreasing by 80% between the historical and EC with dust and 63% without. Though dust impacts influence the rainfall declines significantly between the MC ERS average and EC ERS average, climate perturbations have a more significant impact. Rainfall decreases about 11% between early rainfall season MC and EC in ‘dust on’ simulations, but there is about a 20% decrease in rainfall for ‘dust off’ simulations.

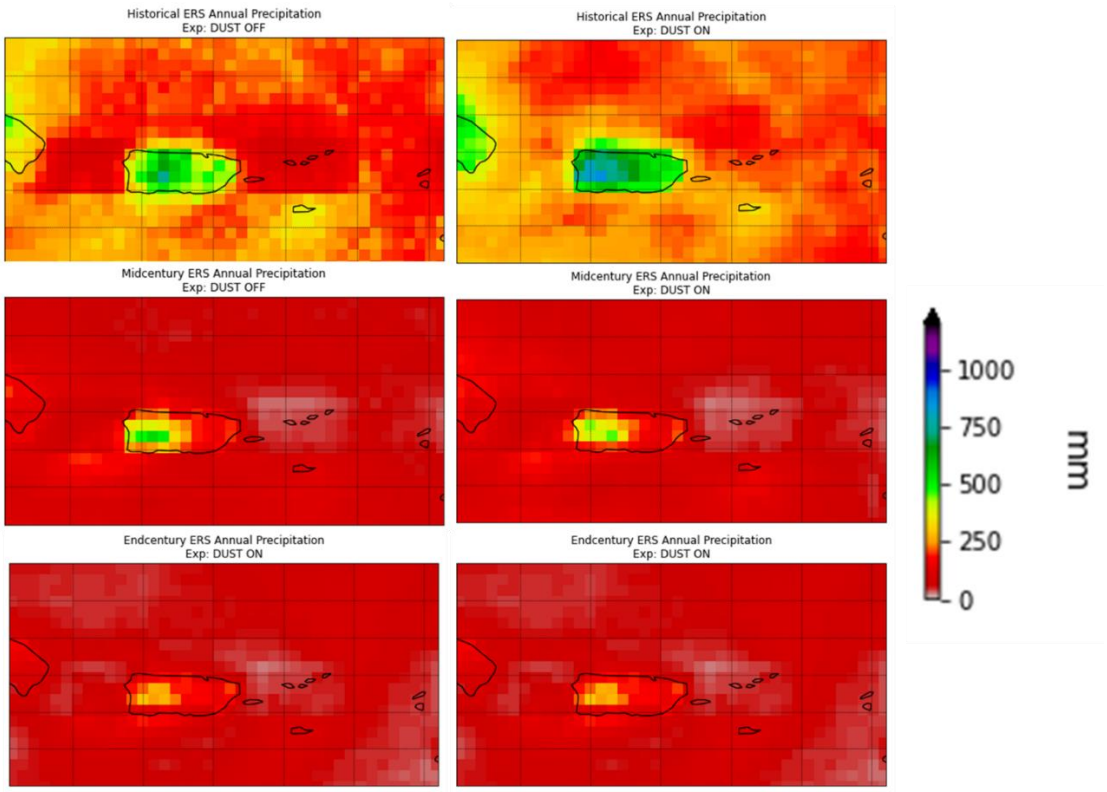

Figure 16. ERS rainfall for all analysis periods. Left: ‘dust off’ simulations; right: ‘dust on’ simulation.

5.5.2 GDI

GDI is useful in determining thermodynamic signatures of the SAL, like mid-tropospheric warming and enhanced stability (Miller et al., 2017). Positive GDI values indicate instability and greater potential for convective storm development, while negative values indicate greater stability and possible subsidence inversion. Though separate from rainfall, GDI values do not show normality. A Wilcox test is again used because the data are non-parametric. Much like the rainfall, historical early rainfall season GDI is over simulated in the ‘dust on’ simulation. The dust has a significant influence on the convection as well. Within the LUQ region, the ‘dust on’

GDI reflected a slightly more convective environment than the ‘dust off’. Though both simulation values reflected short-lived rainfall events are most likely, the ‘dust on’ value indicated more potential for scattered thunderstorm development (Fig. 17). LUQ GDI value decreases over 100% by the MC and an additional 29% between the MC and EC in both simulations.

GDI becomes increasingly negative in the future for both ‘dust on’ and ‘dust off’ simulations annually and in the ERS. Rainfall will be suppressed due to decreased convective development in the western Atlantic. The transition from many shallow and isolated thunderstorms to a strong subsidence inversion is likely induced by the rising atmospheric pressure. Eastern Puerto Rico convection declines faster than the western portion of the island, making the LUQ a region impacted by the mid-century. Monthly averages of GDI over the periods show that the greatest changes in stability occur during March, April, July, and August. Synoptic environment averages suggest that atmospheric patterns set during April intensify through the ERS. The maximum GDI for all periods is in May and June. Mid- and end-century GDI for May and June have the least spatial change in the thermodynamic stability.

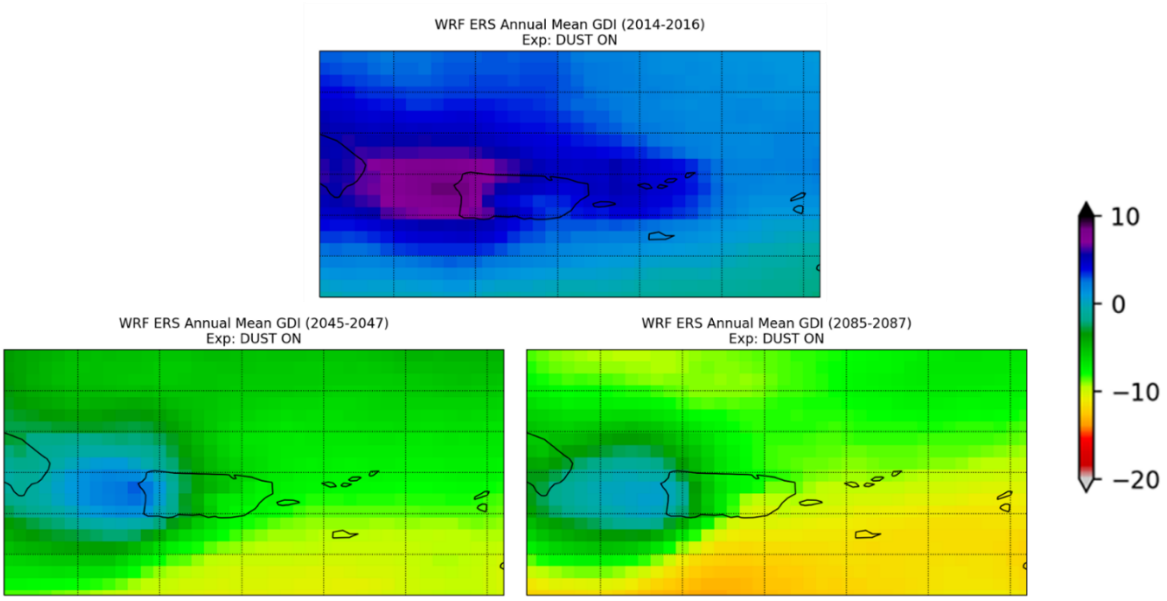

Figure 17. Galvez-Davison Index values averaged over the ERS months for the historical period, MC and EC.

5.5.3 Vapor Pressure Deficit

VPD is the only hydrometeorological variable in this analysis that was normally distributed. As such, a paired t-test is conducted for all analysis periods. Historical and end-century ERS VPD were significantly different in the ‘dust on’ and ‘dust off’ simulations. Conversely, mid-century VPD means are the same in the two simulations, indicated by an accepted null hypothesis with a p-value equal to 0.09. VPD supports rainfall estimates in that conditions are similar for MC ‘dust on’ and ‘dust off’ simulations. The ‘dust on’ and ‘dust off’ VPD output differed most in the historical period. This further suggests that the ERS environment induced by the RCP8.5 scenario has an equal or greater hydrologic impact than dust.

Both simulations agree that majority of the surface will be more saturated in the future, except for areas in southwest Puerto Rico. Rising air temperatures in the future will increase the saturation vapor pressure, so future VPD would be expected to be higher than the historical period. Since the opposite was modeled at the surface (950 hPa), two factors could be influencing model saturation vapor pressure. First, the model uses a climatology for the land surface, including greening periods for vegetation, soil properties, and land use designation. Regardless of atmospheric changes impacting these inputs, all periods use the same land use climatology from MODIS. Secondly, trade winds will continue to bring tropical moisture over PR. Considering warming and rainfall decreases in eastern PR, the land surface model slows plant function, and the atmosphere retains the advected moisture. This leads to the EC's 10–12% increase in atmospheric saturation. In southwest PR, the surface is predicted to be less saturated in the future, with the demand increasing by 7–11% by the EC. The region of higher atmospheric moisture demand corresponds to the area that consistently features higher rainfall and greater potential for storm development. The higher temperatures again play a role in saturation vapor pressure, but because precipitation occurs more often in this region, the land surface model increases evapotranspiration in periods. This leads to increased demand when rainfall is not occurring.

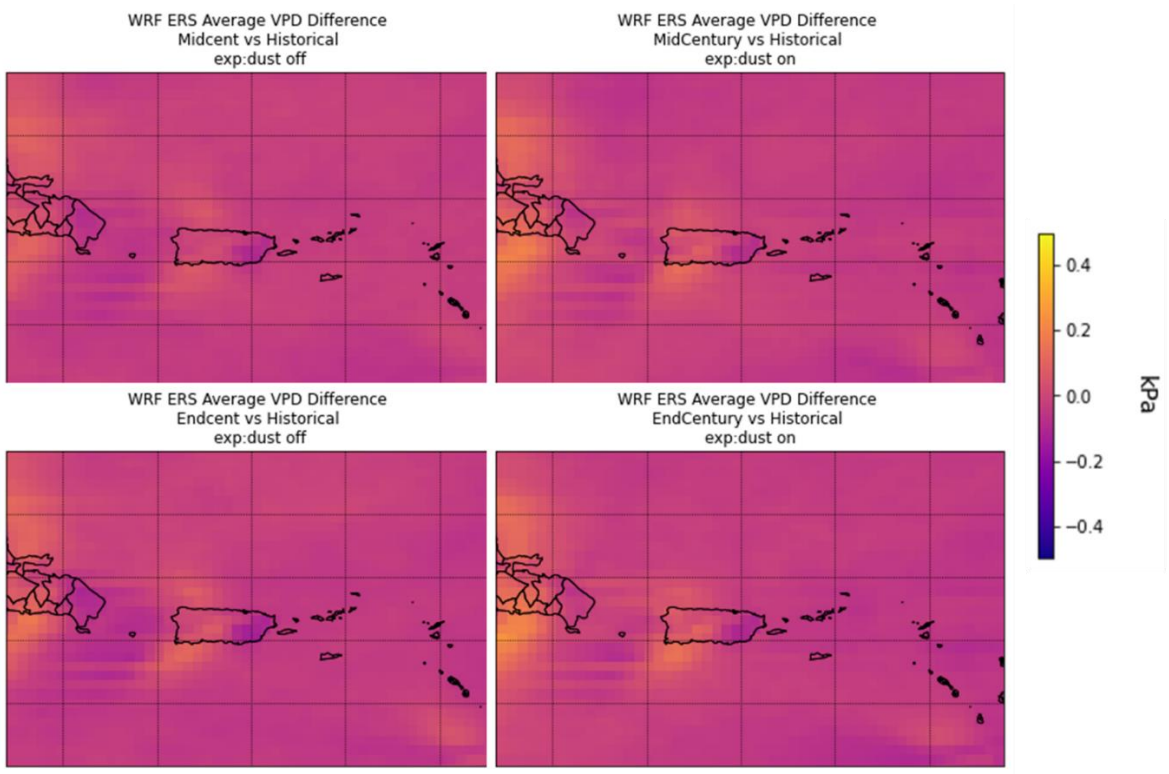

Figure 18. Mid-century and end-century ERS VPD differences from Historical.

5.5.4 Drought Connections

Dynamic downscaling was effective at capturing historical and future thermodynamic influences of dust. Hydrometeorological variables that are influenced by dust and can indicate drought potential were analyzed for three-year periods. Warming introduces early rainfall season rainfall declines that are exacerbated by dust through the mid-century. The mid-century dusty period moisture environment supports similarities in considering greater radiative forcing and greater radiative forcing with emissions. Dust may be important in convective development in the mid and end centuries, but the spatial heterogeneity in Puerto Rico's landscape is significant to the moisture environment changes. Frequently shallow convective rainfall events, increase the vapor pressure demand, and indicate possible frequent local droughts. Eastern Puerto Rico is

more likely to experience widespread drought as evaporation is greater than rainfall. These connections are explored further in Chapters 6 and 7.

CHAPTER 6

Discussion

Future simulations using RCP 8.5 have higher temperatures and greater carbon dioxide loading. Rising atmospheric height related to climate warming does amplify the North Atlantic Sub-tropical High (NASH). Doherty et al. (2008) related increased dust levels in the Caribbean to a westward displacement of the NASH that moves dust from the African coast, similar to the long-term pattern that emerges in the future. They noted that dust was typically transported from the Sahara region only during these times. Model analyses of the historical early rainfall season (ERS) shows a westward place NASH with the highest ERS average aerosol optical depth (AOD) centered over the Sahara. The future ERS synoptic environment does not displace the center of the NASH from its historical ERS position, which aids in Puerto Rico's ERS mean AOD being 0.2 for all periods. Instead, the strength of the NASH controls the transport pathway, and future dust is entrained from the Sahara and Sahel regions (Fig. B11). Transport from the Sahel seems to be directly related to trade wind increases (Fig. 12), while the sub-tropical high location induces transport from the Sahara (Fig. 11). Higher windspeeds in the central tropical Atlantic further assist the transport by keeping aerosols within the SAL. This study's monthly AOD time series show elevated dry season AOD levels compared to Fig. 4 from Doherty et al. (2008). Comparing Doherty et al. (2008)'s 1988–1992 monthly AOD to the modeled historical AOD shows the 2014–2018 peak is two months later. In the future, the peak season will be longer than the 1988–1992 and 2014–2018 seasons.

The AOD analysis is limited by the model's ability to represent the land surface. As previously mentioned, land use and drought significantly influence the Sahara landscape, so dust emission regions could be misrepresented in the future because the landscape is not dynamic in WRF. The AOD portion of this work relied on 64 km output because the dynamic downscale within WRF did not capture the domain 1 dust. This limited the overall analysis, as a correlation between AOD and moisture would be limited. Moisture values would be based on the average of 90 pixels, while AOD would be three pixels. An addition routine, convert_emiss.exe, should have been run before WRF's dynamic downscaling routine called ndown. Convert_emiss.exe preforms the interpolation of emissions from the coarse model output to ensure grid mapping is conserved correctly. The requirement for emissions mapping was unknown before reaching post-processing. 16 km and 4 km resolution dust would improve this analysis. Still, the synoptic level analysis is a valuable predictor of the ability of dust to be transported into the Caribbean during future early rainfall seasons.

The western Caribbean, more specifically Puerto Rico and the US Virgin Islands, are expected to experience up to 327% more dry days through the end of the century (Gutiérrez, et al., 2021). A 16 km resolution could not resolve local effects like orographic rainfall from the Luquillo Mountains, but GDI values did convey the potential for shallow convection along mountainous areas in the western and eastern portions of the island. Jury (2022) found increasing evaporation at the same rate as rainfall received in the western Puerto Rico, indicating moisture recycling similar to the VPD relationship discussed in 5.5.3. Projections for eastern Puerto Rico, where Luquillo is located, are less clear. The surface VPD changes correspond to the arid environment that is predicted in the future (Gutiérrez et al., 2021). In areas that maintain

moisture on the eastern side of the island, much of the water vapor may not be recycled as rainfall. This may lead to evaporation and rainfall imbalances that cause long-term drought.

Recent work by Gutleben et al. (2022) analyzed winter dry season transport of dust into the Caribbean. The key findings of this analysis were that winter dust remained near the marine boundary layer and was always found with water vapor, smoke, and other aerosols. Even during the dry season, aerosol radiative effects are induced that impact shallow cloud processes. These results become interesting when considering a deepened marine boundary layer and greater aerosol concentration in RCP 8.5 simulations. The dust limited the warming effect of carbon dioxide at the surface, resulting in wetter conditions in the future ‘dust on’ analysis.

CHAPTER 7

Conclusion

Puerto Rico is a groundwater-limited island in the eastern Caribbean. Plants, people, and animals on the island depend on large-scale convection and rainfall for daily water needs. The northeastern portion of the island features the Luquillo Mountains, the only remaining tropical rainforest on the island. The geographical location in relation to the trade winds and mountain peak heights has historically made the Luquillo Mountains the wettest location in Puerto Rico (Gómez-Gómez et al., 2014). A stabilized normal climate is critical for the plant and animal species of the rainforest (Zinnert et al., 2021). Deviations in precipitation normal could decrease the water available within and downstream of the Luquillo Mountains (Zinnert et al., 2021). Decreased rainfall was evidenced in 1976–77, 1993–95, and 2015–16, and Earth System Models suggest future declines in annual precipitation for the Caribbean (Larsen, 2000; Hartmann et al., 2013).

During the reduced precipitation periods, drought was induced. Droughts are expected to increase in Puerto Rico due to warming temperatures and rainfall declines, but the mechanisms that will control the early rainfall season declines have not been thoroughly investigated. One factor that enhanced precipitation perturbations was the presence of the SAL (Mote et al., 2017). While dust interacts with the atmosphere and oceans in various ways, the Saharan Air Layer (SAL) is very dry and warm. It can extend through a broad layer of the atmosphere, reducing moisture by limiting water vapor bonding processes (Fig. 3; Dunion, 2011; Reid et al., 2002).

The warm layer also stabilizes the atmosphere, reducing the updraft necessary for cloud formation.

This thesis answered two questions:

- How will the dust intrusion period be affected by anthropogenic warming of the oceans in the Tropical Atlantic?
- How does the seasonality and duration of dust intrusion affect water resources in Puerto Rico, specifically the Luquillo Mountains?

A historical period from 2014 to 2018 or 2014 to 2016 served as the baseline climatology to analyze AOD and water-related variables, respectively. Future periods from 2045 to 2049 (2045 to 2047), described as the mid-century, and 2085 to 2089 (2085 to 2087), described as the end-century, used boundary conditions from CMIP5 RCP8.5 to represent the weather under higher sea surface temperatures. Mean monthly values were compared spatially and temporally across the years to quantify Aerosol Optical Depth (AOD) changes over time. The early rainfall season thermodynamic influence of dust was then analyzed with the Gálvez-Davison Index (GDI). To further convey the thermodynamic changes, total rainfall and vapor pressure deficit are analyzed to determine how water resources are impacted.

Dust transport from the Sahel to the Caribbean is controlled by trade winds over Northern Africa, North Atlantic Oscillation (NAO), and El Nino (Prospero & Mayol-Bracero, 2013). Positive NAO increases the strength of the NASH, which subsequently increases speeds in the trade wind over the Tropical North Atlantic (Herrera et al., 2020). Westward placement of the Atlantic sub-tropical high is associated with dust transport from the Sahara to the Caribbean. Increased strength and a westward placement of NASH create an environment conducive to transporting dust into the Caribbean during the early rainfall season (ERS) through the mid-

summer drought (MSD). This influence is the strongest during the mid-century. Anomalous westerly winds at 700 hPa during the ERS and 850 hPa during the MSD drive higher peak AOD. Changes in the synoptic environment extend through the troposphere. Historical June 500 hPa analysis showed a trough extended from western Europe that supported northeasterly wind movement in the central tropical Atlantic. Future simulations suggest winds June 500 hPa winds are easterly. During both the mid- and end- century wind speeds are higher and easterly, suggesting that the SAL reaches 500 hPa heights and transport from the Sahel will occur in the MSD.

Along with the increased chance of dust outbreaks during the ERS, aerosols remain aloft for more extended periods in the absence of rainfall in the future. The presence of the dust particles significantly affects the moisture environment, although changes in moisture associated with increased CO2 under RCP 8.5 also considerably impact the moisture. During the Mid-century, these aerosols equally lead to decreases in water availability, signifying that the cooling effect of dust will play a critical role in a warmer climate. This detail will be important as Saharan dust emission predictions can be made more confidently.

The LUQ will be significantly impacted by future droughts and experience annual and ERS rainfall means less than historically recorded. Though atmospheric moisture may still be available, convection is limited by increased stability from mid-tropospheric warming due to changes in CO2 and dust aerosols. Shallow daily convection may persist and assist in the tropical forest's resistance to drying. Simulations combining both dust effects and a warmer climate reflect a wetter Luquillo. Still, the declines on the island's eastern side are sharper than those on the western. Nonetheless, island-wide reductions occur, with the mean percent change from the historical to MC being 69% ('dust on') and 52% ('dust off').

Future work should first produce a 5-yr analysis for the moisture variables. There are plans to dynamically downscale to 4 km, but before that is undertaken, 16 km simulations should be re-run with the emissions mapped. To downscale emissions output, convert_emiss with the namelist prep_chem_sources should be executed before running ndown. Though this 64 and 16 km analysis well represented the historical and future dust and moisture environments of Puerto Rico, the combination of higher resolution data and a complete vertical analysis will benefit Luquillo management. The synoptic analysis can be enhanced by using an average of the SAL rather than analyzing layers typically at the top and bottom separately. The GDI component for the inversion index and mid-level warming can also be explored along with GDI at monthly scales to understand the moisture and temperature relationship through the layer. Spatially precise cooling and warming effects of dust can be assessed, as well as the response within the tropical rainforest because local processes can be reflected in greater detail.

References

Adebiyi, A. A., & Kok, J. F. (2020). Climate models miss most of the coarse dust in the atmosphere. *Science Advances, 6*, eeaz9507. doi: 10.1126/sciadv.aaz9507.

Albani, S. & Mahowald, N. M. (2019). Paleodust insights into dust impacts on climate. *Journal of Climate, 32*(22). 7897–7913. doi:10.1175/JCLI-D-18-0742.1.

Angeles, M.E., J. E. González, N. D. Ramírez-Beltrán, C. A. Tepley, and D. E. Comarazamy. (2010). Origins of the Caribbean rainfall bimodal behavior. *Journal of Geophysical Research, 115*, D11106. doi:10.1029/2009JD012990.

Arias, P.A., & 75 others (2021). Technical Summary. In Climate Change 2021: The Physical Science Basis. Contribution of Working Group I to the Sixth Assessment Report of the Intergovernmental Panel on Climate Change [Masson-Delmotte, V., P. Zhai, A. Pirani, S.L. Connors, C. Péan, S. Berger, N. Caud, Y. Chen, L. Goldfarb, M.I. Gomis, M. Huang, K. Leitzell, E. Lonnoy, J.B.R. Matthews, T.K. Maycock, T. Waterfield, O. Yelekçi, R. Yu, and B. Zhou (eds.)]. Cambridge University Press, Cambridge, United Kingdom and New York, NY, USA, pp. 33−144. doi:10.1017/9781009157896.002.

Ashby, S. A., Taylor, M. A., & Chen, A. A. (2005). Statistical models for predicting rainfall in the Caribbean. *Theoretical and Applied Climatology, 82*(1), 65–80. doi:10.1007/s00704-004-0118-8.

Ault, T. (2020). On the essentials of drought in a changing climate. *Science, 368*(6488), 256–260. doi:10.1126/science.aaz5492.

Barkan, J., Kutiel, H., Alpert, P., & Kishcha, P. (2004). Synoptics of dust intrusion days from the african continent into the Atlantic ocean. *Journal of Geophysical Research: Atmospheres, 109*(D8), D08201. doi:10.1029/2003JD004416.

Barkhordarian, A., Saatchi, S.S., Behrangi, A., Loikith, P. C., & Mechoso, C. R. (2019). A recent systematic increase in vapor pressure deficit over tropical South America. *Scientific Reports, 9*, 15331. doi:10.1038/s41598-019-51857-8.

Charlery, J., Nurse, L., & Whitehall, K. (2006) Exploring the relationship between the North Atlantic oscillation and rainfall patterns in Barbados. *International Journal of Climatology*, *26*, 819–827.

Chen, S., Huang, C., Kuo, Y., Tseng, Y., Gu, Y., Earl, K., Chen, C.-Y., Choi, Y. & Liou, K. (2021). Impacts of Saharan mineral dust on Air-Sea interaction over north Atlantic Ocean using a fully coupled regional model. *Journal of Geophysical Research: Atmospheres, 126(4)*, e2020JD033586. doi:10.1029/2020jd033586.

Chen, A., & Taylor, M. A. (2002). Investigating the link between early season Caribbean rainfall and the El Niño + 1 year. *International Journal of Climatology*, *22*, 87–106.

Chiapello, I., Bergametti, G., Gomes, L., Chatenet, B., Dulac, F., Pimenta, J., & Suares, E. S. (1995). An additional low layer transport of Sahelian and Saharan dust over the North-Eastern Tropical Atlantic. *Geophysical Research Letters, 22(23)*, 3191–3194. doi:10.1029/95GL03313.

Dai, A. (2013). Increasing drought under global warming in observations and models. *National Climate Change, 3*, 52–58. doi:10.1038/nclimate1633.

Dai, A. & Zhao, T. (2017). Uncertainties in historical changes and future projections of drought. Part I: Estimates of historical drought changes. *Climatic Change, 144,* 519–533. doi:10.1007/s10584-016-1705-2.

Doherty, O. M., Riermer, N., Hameed, S. (2008). Saharan mineral dust transport into the Caribbean: observed atmospheric controls and trends. *Journal of Geophysical Research, 113*, D07211. doi:10.1029/2007JD009171.

Dunion, J.P. (2011). Re-Writing the climatology of the tropical North Atlantic and Caribbean Sea atmosphere. *Journal of Climate.*, *24*, 893–908.

Evan, A. T., Foltz, G. R., Zhang, D., & Vimont, D. J. (2011). Influence of African dust on ocean-atmosphere variability in the tropical Atlantic. *Nature Geoscience, 4(11),* 762–765. doi:10.1038/NGEO1276.

Flaounas, E., Kotroni, V., Lagouvardos, K., Klose, M., Flamant, C., & Giannaros, T. M. (2017). Sensitivity of the WRF-Chem (V3.6.1) model to different dust emission parametrisation: Assessment in the broader Mediterranean region. *Geoscientific Model Development, 10(8),* 2925–2945. doi:10.5194/gmd-10-2925-2017.

Foster, P. (2001). The potential negative impacts of global climate change on tropical montane cloud forests. *Earth-Science Reviews, 55,* 73–106.

Gálvez, J. M., & Davison, M. (2016). The Gálvez-Davison Index for tropical convection, accessed 10 July 2017. Retrieved from: http://www.wpc.ncep.noaa.gov/international/gdi/GDI_Manuscript_V20161021.pdf

Gamble, D. W., & Curtis, S. (2008). Caribbean precipitation: Review, model and prospect. *Progress in Physical Geography, 32(3),* 265–276. doi:10.1177/0309133308096027.

Giannini, A., Kushnir, Y. &. Cane, M. A. (2000). Interannual variability of Caribbean rainfall, ENSO, and the Atlantic Ocean. *Journal of Climate, 13*, 297–311.

Ginoux, P., Prospero, J. M., Torres, O. & Chin, M. (2004). Long-term simulation of global dust distribution with the GOCART model: Correlation with the North Atlantic Oscillation. *Environmental Modelling & Software, 19*, 113–128. doi:10.1016/S1364-8152(03)00114-2.

Gioda, A., Mayol-Bracero, O. L., Scatena, F. N., Weathers, K. C., Mateus, V. L., & McDowell, W. H. (2013). Chemical constituents in clouds and rainwater in the Puerto Rican rainforest: Potential sources and seasonal drivers. *Atmospheric Environment, 68*, 208–220. doi:10.1016/j.atmosenv.2012.11.017.

Gómez-Gómez, F., Rodríguez-Martínez, J., & Santiago, M. (2014). *Hydrogeology of Puerto Rico and the outlying islands of Vieques, Culebra, and Mona*. United States Geological Survey & United States Department of the Interior. https://pubs.usgs.gov/sim/3296/pdf/sim3296.pdf

Gutiérrez, J.M., R.G. Jones, G.T. Narisma, L.M. Alves, M. Amjad, I.V. Gorodetskaya, M. Grose, N.A.B. Klutse, S. Krakovska, J. Li, D. Martínez-Castro, L.O. Mearns, S.H. Mernild, T. Ngo-Duc, B. van den Hurk, and J.-H. Yoon (2021). Atlas. In Climate Change 2021: The Physical Science Basis. Contribution of Working Group I to the Sixth Assessment Report of the Intergovernmental Panel on Climate Change [Masson-Delmotte, V., P. Zhai, A. Pirani, S.L. Connors, C. Péan, S. Berger, N. Caud, Y. Chen, L. Goldfarb, M.I. Gomis, M. Huang, K. Leitzell, E. Lonnoy, J.B.R. Matthews, T.K. Maycock, T. Waterfield, O. Yelekçi, R. Yu, and B. Zhou (eds.)]. Cambridge University Press, Cambridge, United Kingdom and New York, NY, USA, pp. 1927–2058. doi:10.1017/9781009157896.021.

Gutleben, M., Groß, S., Heske, C., & Wirth, M. (2022). Wintertime Saharan dust transport towards the Caribbean: An airborne lidar case study during EUREC4A Copernicus GmbH, *Atmospheric Chemistry and Physics*, *22*, 7319–7330. doi:10.5194/acp-22-7319-2022

Hartmann, D.L., A.M.G. Klein Tank, M. Rusticucci, L.V. Alexander, S. Brönnimann, Y. Charabi, F.J. Dentener, E.J. Dlugokencky, D.R. Easterling, A. Kaplan, B.J. Soden, P.W. Thorne, M. Wild and P.M. Zhai, 2013: Observations: Atmosphere and Surface. In: Climate Change 2013: The Physical Science Basis. Contribution of Working Group I to the Fifth Assessment Report of the Intergovernmental Panel on Climate Change [Stocker, T.F., D. Qin, G.-K. Plattner, M. Tignor, S.K. Allen, J. Boschung, A. Nauels, Y. Xia, V. Bex and P.M. Midgley (eds.)]. Cambridge University Press, Cambridge, United Kingdom and New York, NY, USA.

Herrera, D. & Ault, T. (2017). Insights from a new high-resolution drought atlas for the Caribbean spanning 1950–2016. *Journal of Climate*, *30(19),* 7801–7825. doi:10.1175/JCLI-D-16-0838.1.

Huffman, G.J., E.F. Stocker, D.T. Bolvin, E.J. Nelkin, Jackson Tan (2019), GPM IMERG Final Precipitation L3 1 month 0.1 degree x 0.1 degree V06, Greenbelt, MD, Goddard Earth Sciences Data and Information Services Center (GES DISC), Accessed: February 2, 2022. doi:10.5067/GPM/IMERG/3B-MONTH/06.

Jordan, A. K., Gnanadesikan, A., & Zaitchik, B. (2018). Simulated dust aerosol impacts on western Sahelian rainfall: Importance of Ocean Coupling. *Journal of Climate, 31*(22), 9107–9124. doi:10.1175/JCLI-D-17-0819.1.

Jury, M., Malmgren, B. A., & Winter, A. (2007). Subregional precipitation climate of the Caribbean and relationships with ENSO and NAO. *Journal of Geophysical Research, 112*, D16107. doi:10.1029/2006JD007541.

Jury, M. R. (2022). Inter-comparison of past and projected climatic trends in Puerto Rico: 1950–2100. *Journal of Water and Climate Change, 13(7)*, 2713–2724. doi:10.2166/wcc.2022.071.

Kohfeld, K. E., & Harrison, S. P. (2001). DIRTMAP: The geological record of dust. *Earth Science Review, 54*, 81–114. doi:10.1016/S0012-8252(01)00042-3.

Larsen, M. C. (2000). Analysis of 20th century rainfall and streamflow to characterize drought and water resources in Puerto Rico. *Physical Geography, 21*, 494–521.

Laurance, W. F., and 52 others (2011). Global warming, elevational ranges and the vulnerability of tropical biota. *Biological Conservation, 144*(1), 548–557. doi:10.1016/j.biocon.2010.10.010.

LeGrand, S. L., Polashenski, C., Letcher, T. W., Creighton, G. A., Peckham, S. E., & Cetola, J. D. (2019). The AFWA dust emission scheme for the GOCART aerosol model in WRF-Chem v3.8.1. *Geoscientific Model Development, 12(1)*, 131–166. doi:10.5194/ gmd-12-131-2019.

Maher, B. A., Prospero, J. M., Mackie, D., Gaiero, D., Hesse, P. P., & Balkanski, Y. (2010). Global connections between aeolian dust, climate and ocean biogeochemistry at the present day and at the last glacial maximum. *Earth-Science Reviews, 99(1)*, 61–97. doi:10.1016/j.earscirev.2009.12.001.

Mahowald, N. M. & Kiehl, L. M. (2003). Mineral aerosol and cloud interactions. *Geophysical Research Letters, 30(9)*, 1475. doi:10.1029/2002GL016762.

Mahowald, N. M., Kloster, S., Engelstaedter, S., Moore, J. K., Mukhopadhyay, S., McConnell, J. R., Albani, S., Doney, S. C., Bhattacharya, A., Curran, M. A. J., Flanner, M. G., Hoffman, F. M., Lawrence, D. M., Lindsay, K., Mayewski, P. A., Neff, J., Rothenberg, D., Thomas, E., Thornton, P. E., and Zender, C. S. (2010). Observed 20th Century desert dust variability: Impact on climate and biogeochemistry. *Atmospheric Chemistry and Physics, 10*, 10875–10893, doi:10.5194/acp-10-10875-2010.

Malmgren, B. A., Winter, A., & Chen, D. (1998). El Niño–Southern Oscillation and North Atlantic Oscillation control of climate in Puerto Rico. *Journal of Climate, 11(10)*, 2713–2717. doi:10.1175/1520-0442(1998)011%3C2713:ENOSOA%3E2.0.CO;2.

Martin, P. H., Fahey, T. J. & Sherman R. E. (2011). Vegetation zonation in a neotropical montane forest: Environment, disturbance and ecotones. *Biotropica*, *43*, 533–543.

Martínez-Garcia, A., Rosell-Melé, A., Geibert, W., Gersonde, R., Masqué, P., Gaspari, V., & Barbante, C. (2009). Links between iron supply, marine productivity, sea surface temperature, and CO2 over the last 1.1 ma. *Paleoceanography, 24(1)*, PA1207. doi:10.1029/2008PA001657.

Miller, P. W., Mote, T. L., & Ramseyer, C. A. (2019). An empirical study of the relationship between seasonal precipitation and thermodynamic environment in Puerto Rico. *Weather and Forecasting*, 34, 277–288. doi:10.1175/WAF-D-18-0127.1.

Miller, P. W., & Ramseyer, C. A. (2020). Did the climate forecast system anticipate the 2015 Caribbean drought? *Journal of Hydrometeorology, 21*(6), 1245–1258. doi:10.1175/JHM-D-19-0284.1.

Miller, P. W., Williams, M., & Mote, T. L. (2021). Modeled atmospheric optical and thermodynamic responses to an exceptional Trans-Atlantic dust outbreak. *Journal of Geophysical Research: Atmospheres*, *126*, e2020JD032909. doi:10.1029/2020jd032909.

Molina-Rivera, W.L., and Irizarry-Ortiz, M.M. (2021). Estimated water withdrawals and use in Puerto Rico, 2015: U.S. Geological Survey Open-File Report 2021–1060, 38 p. doi:10.3133/ofr20211060.

Mote, T. L., Ramseyer, C. A., & Miller, P. W. (2017). The Saharan Air Layer as an early rainfall season suppressant in the Eastern Caribbean: The 2015 Puerto Rico drought. *Journal of Geophysical Research: Atmospheres*, *122*, 10966–10982. doi:10.1002/2017JD026911.

National Centers for Environmental Information. (2016). *Drought – Annual 2015*. National Oceanic and Atmospheric Administration. https://www.ncdc.noaa.gov/sotc/drought/201513#pr-sect.

Platnick, S., Hubanks, P., Meyer, K., and King, M. D. (2015). MODIS Atmosphere L3 Monthly Product (08_L3). NASA MODIS Adaptive Processing System, Goddard Space Flight Center. doi:10.5067/MODIS/MOD08_M3.006.

Prospero, J.M. & Lamb, P.J. (2003). African droughts and dust transport to the Caribbean: Climate change implications. *Science*, *302*, 1024–1027. doi:10.1126/science.1089915.

Prospero, J. M. & Mayol-Bracero, O. L. (2013). Understanding the transport and impact of African dust on the Caribbean Basin. *Bulletin of the American Meteorological Society*, *94 (9)*, 1329–1337. doi:10.1175/BAMS-D-12-00142.1.

Ramseyer, C.A. and Mote, T.L. (2018). Analysing regional climate forcing on historical precipitation variability in Northeast Puerto Rico. *International Journal of Climatology*, *38*, e224–e236. doi:10.1002/joc.5364.

Ramseyer, C. A., Miller, P. W., & Mote, T. L. (2019). Future precipitation variability during the early rainfall season in the El Yunque National Forest. *Science of the Total Environment, 661*, 326-336. doi:10.1016/j.scitotenv.2019.01.167.

Reid, J. S., Westphal, D. L., Livingston, M. J., Savoie, D. L., Maring, H. B., Jonsson, H. H., Eleuterio, D. P., Kinney, J. E., & Reid, E. A. (2002). Dust vertical distribution in the Caribbean during the Puerto Rico Dust Experiment. *Geophysical Research Letters, 29 (7)*, 1151. doi:10.1029/2001GL014092.

Schepanski, K., Heinold, B., and Tegen, I. (2017). Harmattan, Saharan heat low, and West African monsoon circulation: Modulations on the Saharan dust outflow towards the North Atlantic. *Atmospheric Chemistry and Physics, 17*, 10223–10243. doi:10.5194/acp-17-10223-2017.

Schwartz, N. B., Budsock, A. M., & Uriarte, M. A. (2019). Fragmentation, forest structure, and topography modulate impacts of drought in a tropical forest landscape. *Ecology, 100(6)*, e02677. doi:10.1002/ecy.2677.

Seneviratne, S.I., N. Nicholls, D. Easterling, C.M. Goodess, S. Kanae, J. Kossin, Y. Luo, J. Marengo, K. McInnes, M. Rahimi, M. Reichstein, A. Sorteberg, C. Vera, and X. Zhang, (2012). Changes in climate extremes and their impacts on the natural physical environment. In: Managing the Risks of Extreme Events and Disasters to Advance Climate Change Adaptation [Field, C.B., V. Barros, T.F. Stocker, D. Qin, D.J. Dokken, K.L. Ebi, M.D. Mastrandrea, K.J. Mach, G.-K. Plattner, S.K. Allen, M. Tignor, and P.M. Midgley (eds.)]. A Special Report of Working Groups I and II of the Intergovernmental Panel on Climate Change (IPCC). Cambridge University Press, Cambridge, UK, and New York, NY, USA, pp. 109–230.

Shao, Y., Wyrwoll, K., Chappell, A., Huang, J., Lin, Z., McTainsh, G. H., Mikami, M., Tanaka, T., Wang, X., & Yoon, S. (2011). Dust cycle: An emerging core theme in Earth system science. *Aeolian Research, 2(4),* 181–204. doi:10.1016/j.aeolia.2011.02.001.

Strong, J. D. O., Vecchi, G. A., & Ginoux, P. (2015). The response of the tropical Atlantic and West African climate to Saharan dust in a fully coupled GCM. *Journal of Climate, 28(18),* 7071–7092. doi:10.1175/JCLI-D-14-00797.1.

Trenberth, K. E. (1997). The definition of El Nino. *Bulletin of the American Meteorological Society, 78,* 2771–2778.

United States Geological Survey (n.d.). *Drought conditions in Puerto Rico*. United States Geological Survey. https://www.usgs.gov/centers/car-fl-water/science/drought-conditions-puerto-rico?qt-science_center_objects=0#qt-science_center_objects

Van Beusekom, A. E., Gonzalez, G. & Scholl, M. A. (2017). Analyzing cloud base at local and regional scales to understand tropical montane cloud forest vulnerability to climate change. *Atmospheric Chemistry and Physics, 17,* 7245–7259. doi: 10.5194/acp-17-7245-2017.

Van der Schrier, G., Barichivich, J., Briffa, K. R., Jones, P. D. (2013). A scPDSI-based global data set of dry and wet spells for 1901-2009. *Journal of Geophysical Research: Atmospheres, 118(10),* 4025–4048. doi:10.1002/jgrd.50355.

Waide, R. B., Comarazamy, D. E., González, J. E., Hall, C. A. S., Lugo, A. E., Luvall, J. C., Murphy, D. J., Ortiz-Zayas, J. R., Ramírez-Beltrán, N. D., Scatena, F. N., Silver, W. L. (2013). Climate variability at multiple spatial and temporal scales in the Luquillo Mountains, Puerto Rico. Pages 21-42 in G. González, M. R. Willig, and R. B. Waide, eds. Ecological gradient analyses in a tropical landscape. Ecological Bulletins 54. Wiley-Blackwell, Hoboken, NJ.

Williams, R. McGee, D., Kinsley, C., Ridley, D., Hu, S., Fedorov, A., Tal, I., Murray, R., & deMenocal, P. (2016). Glacial to Holocene changes in trans-Atlantic Saharan dust transport and dust-climate feedbacks. *Science Advances, 2(11)*. doi: 10.1126/sciadv.1600445.

Wong, S., Colarco, P. R. & Dessler, A. E. (2006). Principal component analysis of the evolution of the Saharan air layer and dust transport: Comparison between a model simulation and MODIS and AIRS retrievals. *Journal of Geophysical. Research*, *111*, D20109. doi:10.1029/2006JD007093.

Wong, S., Dessler, A. E., Mahowald, N. M., Colarco, P. R. & da Silva, A. (2008). Long-term variability in Saharan dust transport and its link to North Atlantic sea surface temperature. *Geophysical Research Letters*, *35*, L07812. doi:10.1029/2007GL032297.

Wu, L. (2007). Impact of Saharan air layer on hurricane peak intensity. *Geophysical Research Letters*, *34*(9). doi:10.1029/2007GL029564.

Yuan, W., and 24 others (2019). Increased atmospheric vapor pressure deficit reduces global vegetation growth. *Science Advances*, *5*(8), eaax1396. doi:10.1126/sciadv.aax1396.

Zhao, T. & Dai, A. (2015). The magnitude and causes of global drought changes in the Twenty-First Century under a low-moderate emissions scenario. *Journal of Climate, 28(11),* 4490–4512. doi:10.1175/JCLI-D-14-00363.1.

Zinnert, J. C., and 22 others (2021). State changes: Insights from the U.S. long term ecological research network. *Ecosphere, 12(5),* e03433. doi:10.1002/ecs2.3433

Appendix A: 2015 Case

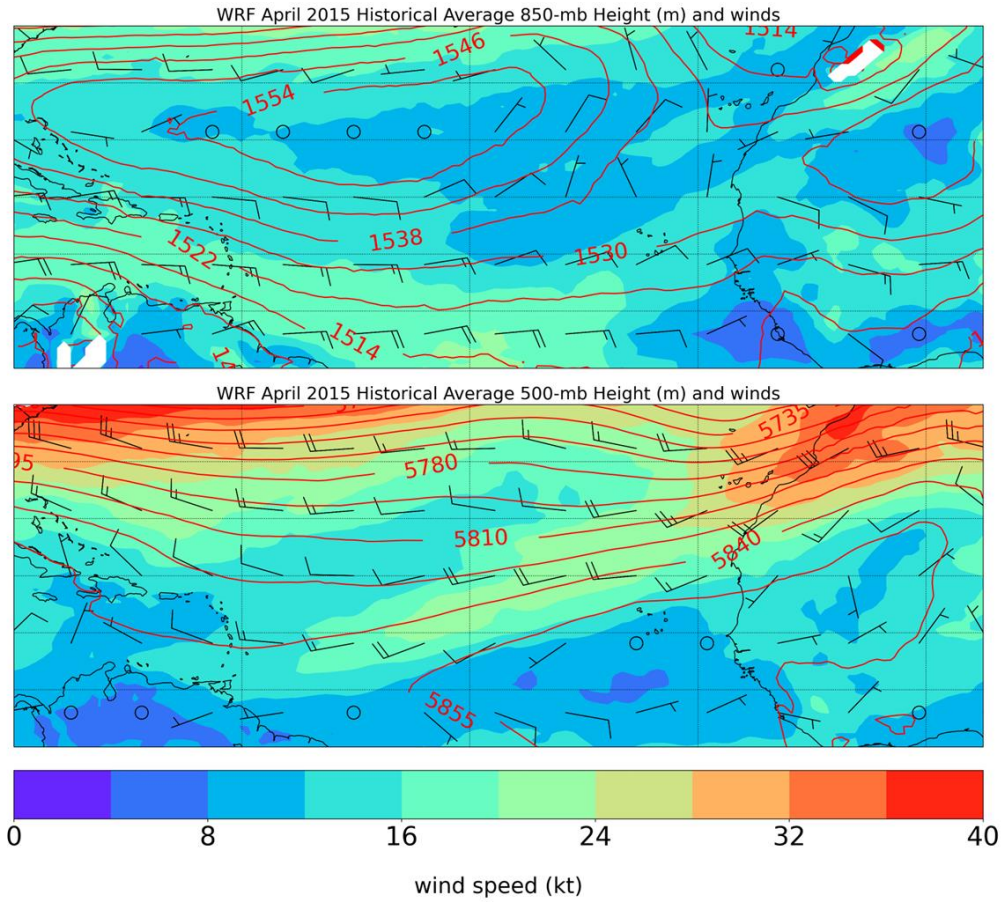

Figure A1. April 2015 500 and 800 hPa heights and winds. Pressure level height is shown in the red contours, wind speed in the filled color contours and wind direction via barbs.

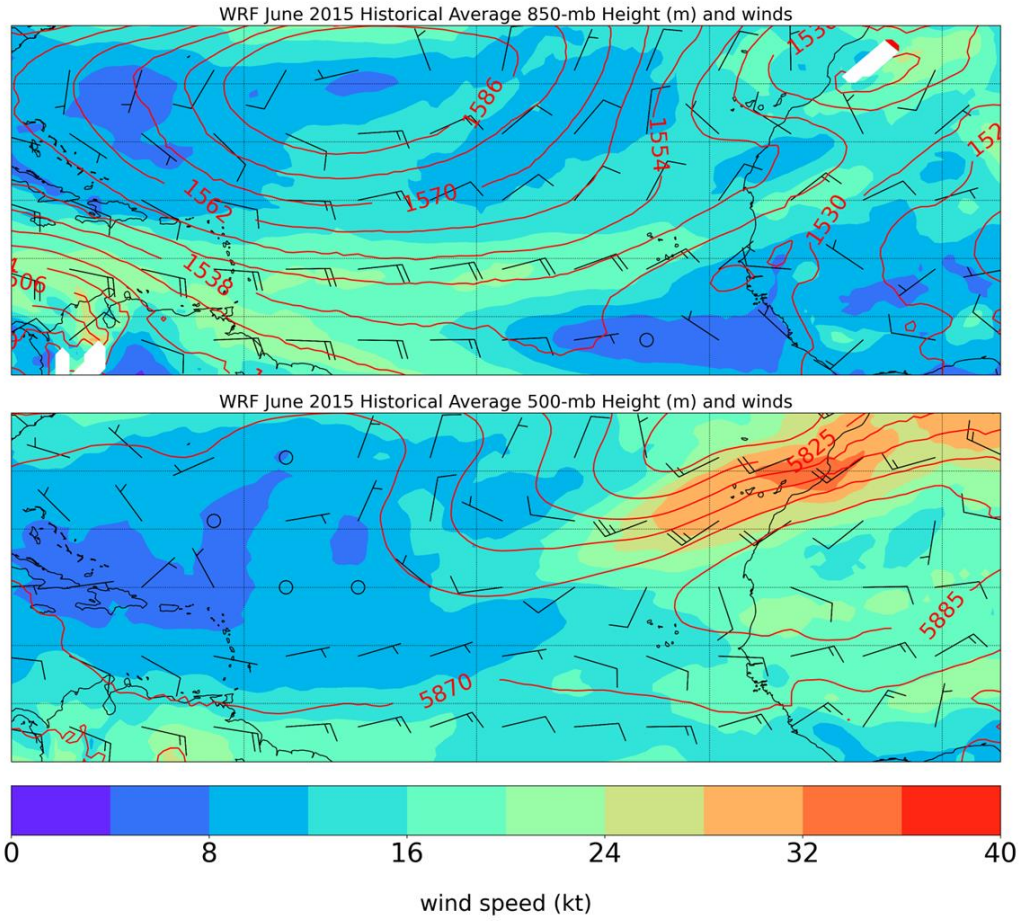

Figure A2. June 2015 500 and 800 hPa heights and winds. Pressure level height is shown in the red contours, wind speed in the filled color contours and wind direction via barbs.

Appendix B: Annual Synoptic Environments

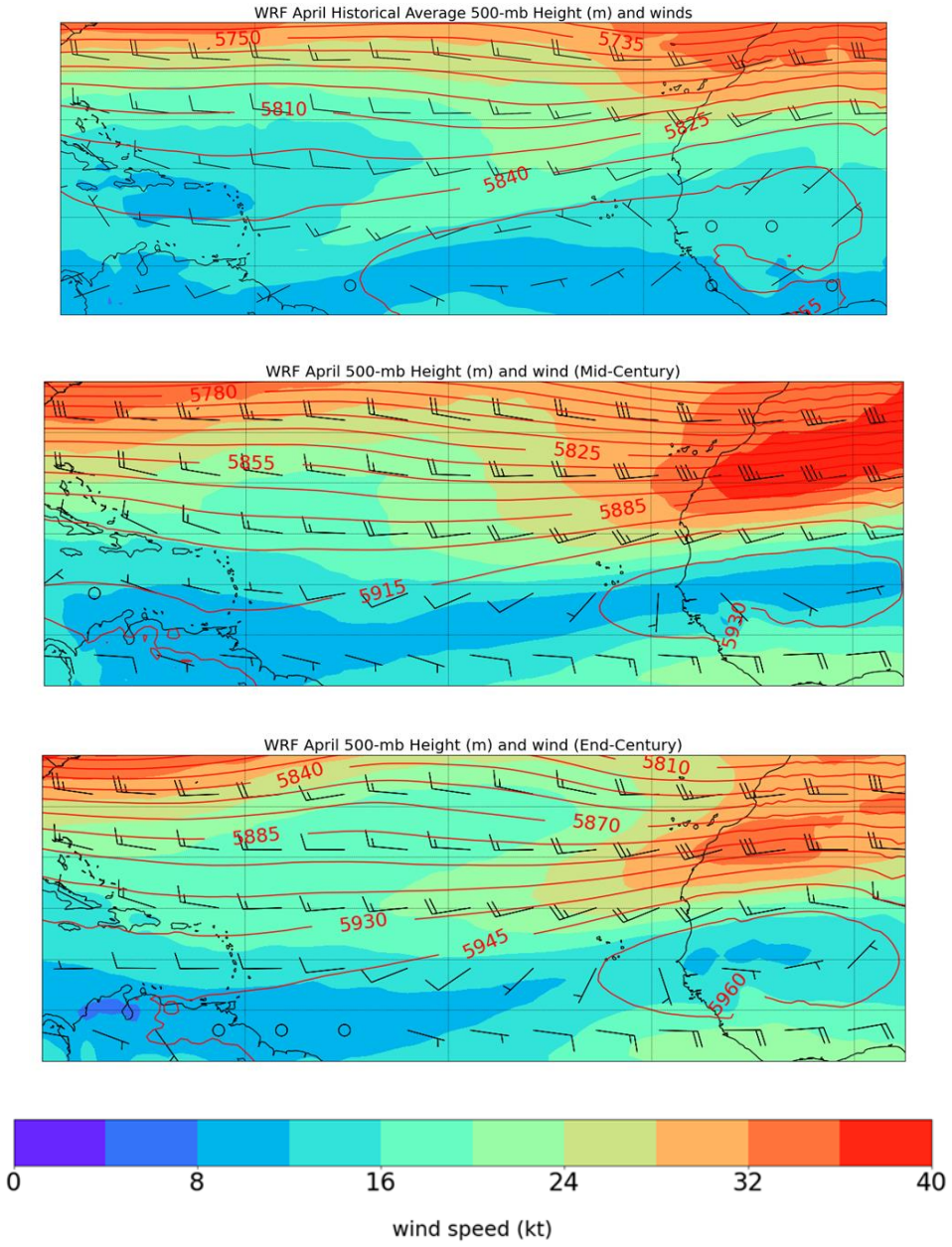

Figure B1. April 500 hPa pressure level heights, wind speed and wind direction for the Historical, IC, and EC.

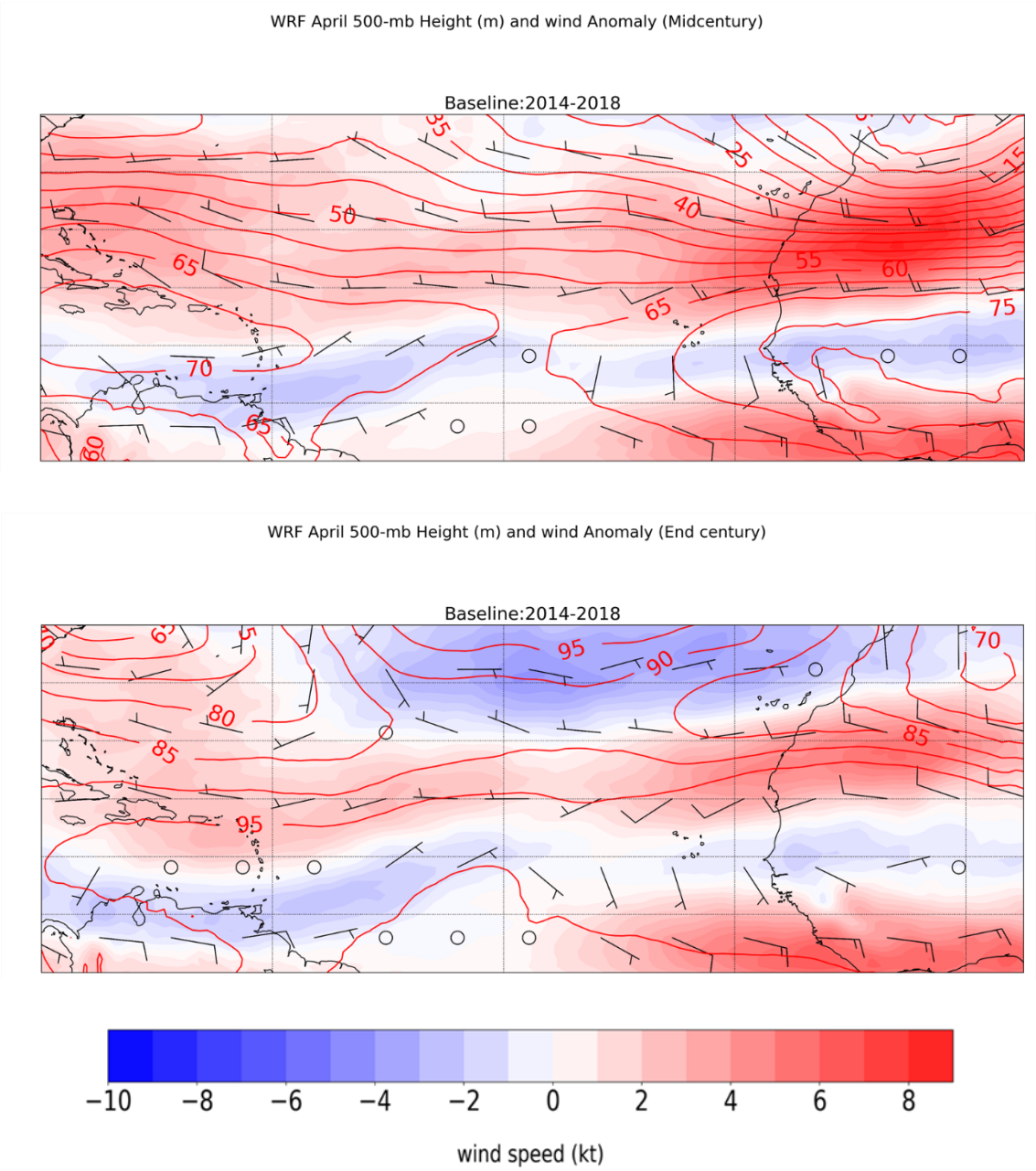

Figure B2. April 500 hPa future anomalies. Positive values indicate higher values in the future period.

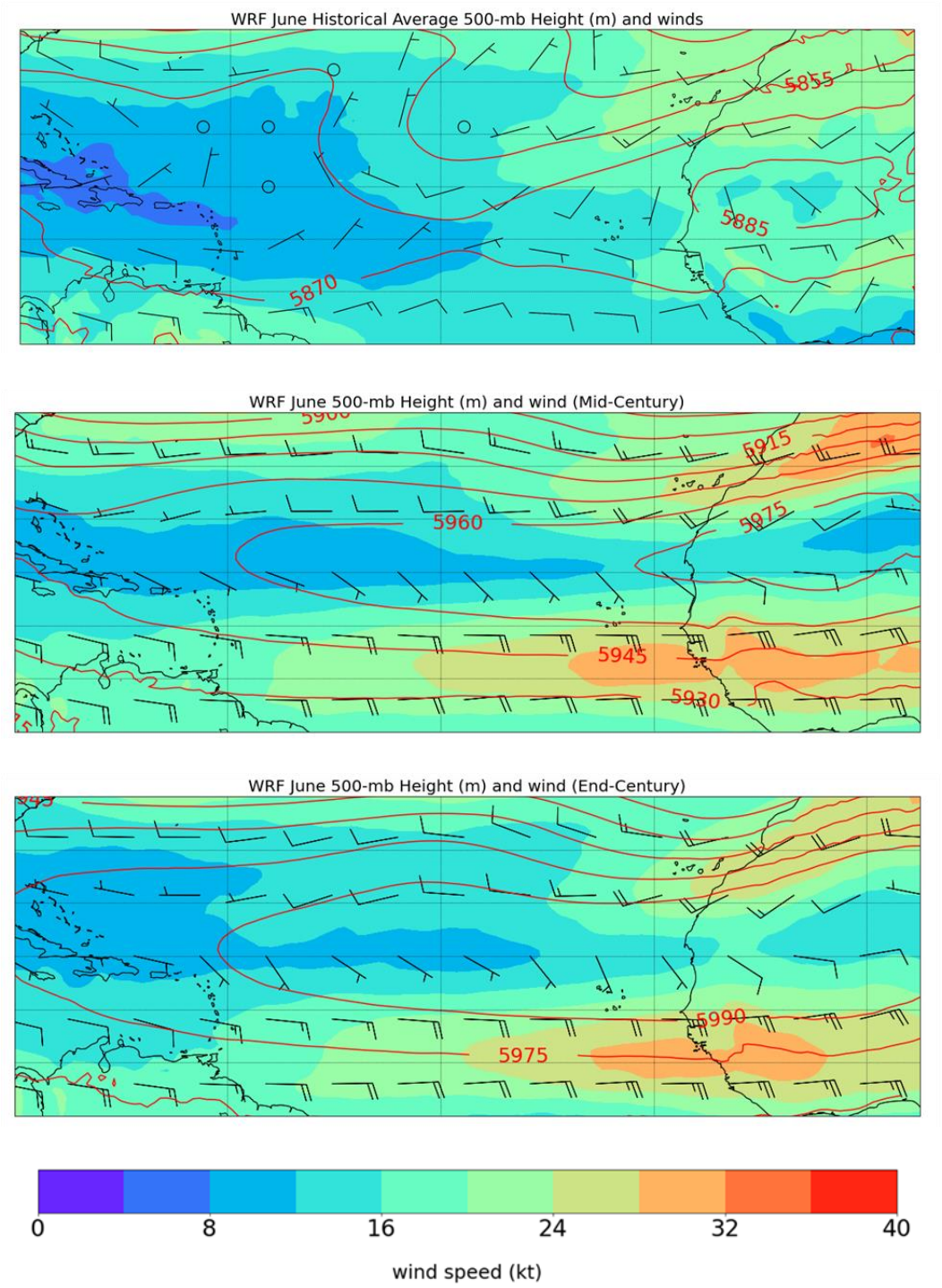

Figure B3. June 500 hPa pressure level heights, wind speed and wind direction for the Historical, IC, and EC.

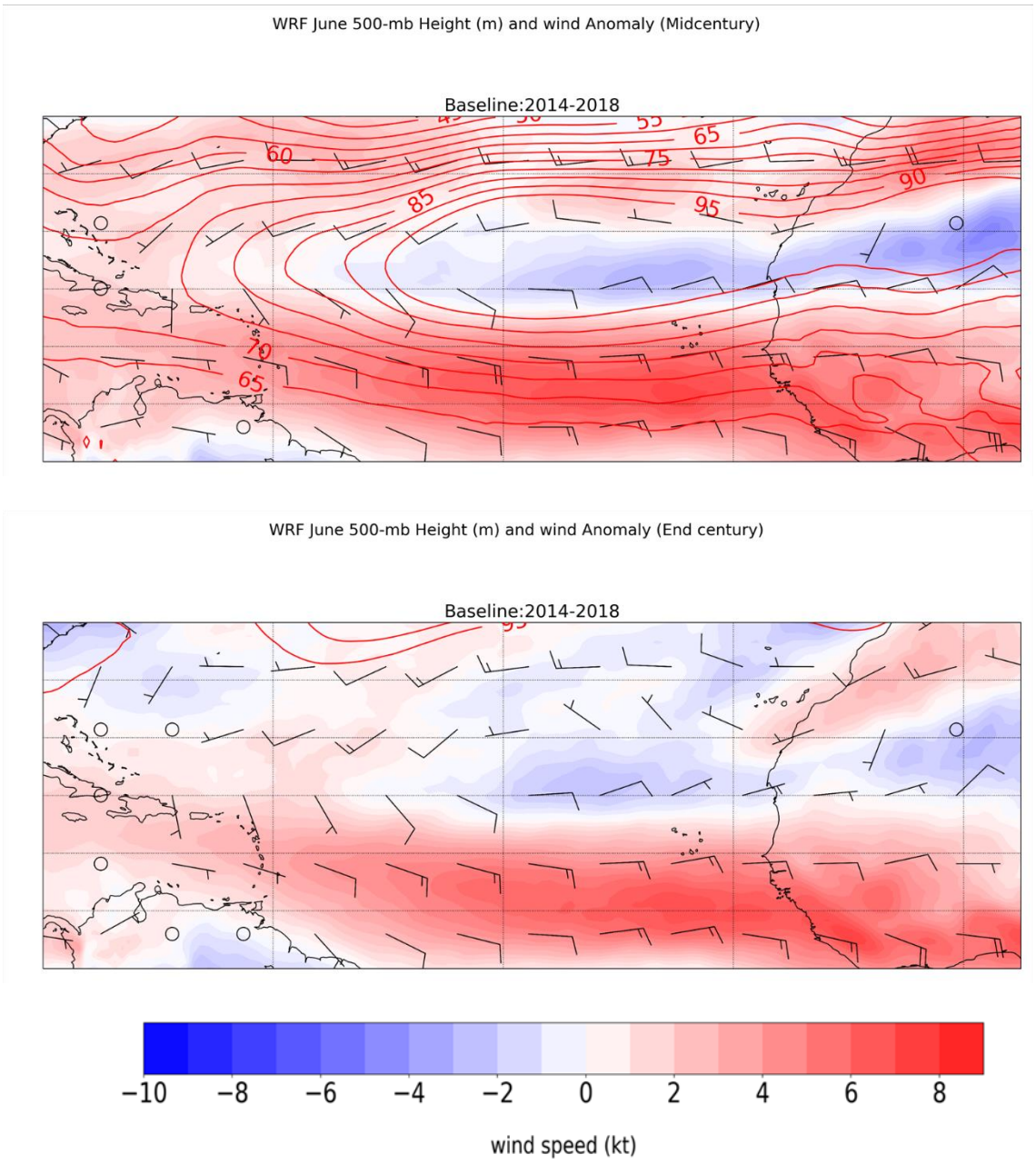

Figure B4. June 500 hPa future anomalies. Positive values indicate higher values in the future period.

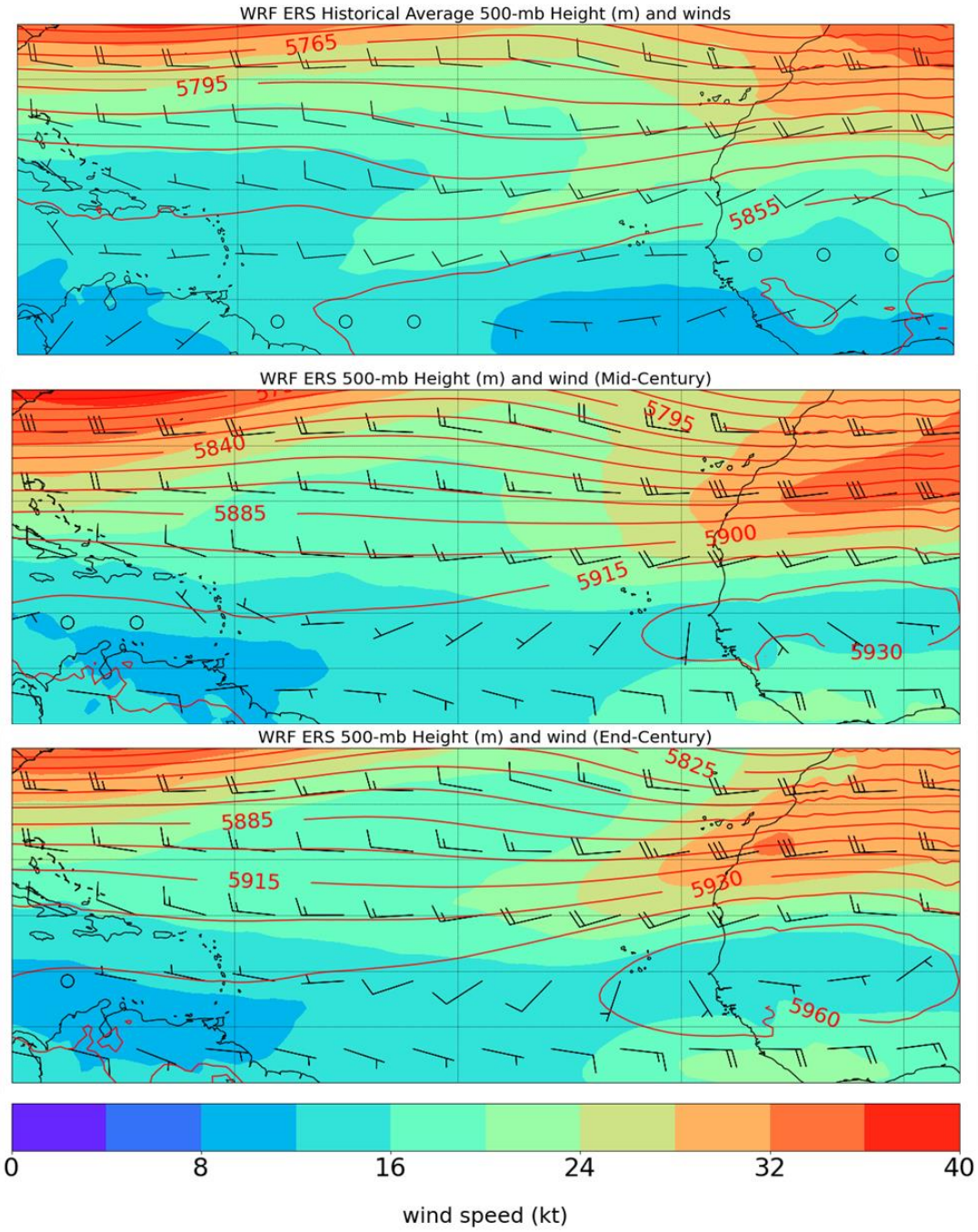

Figure B5**.** ERS annual average heights, wind speed, and direction at 500 hPa.

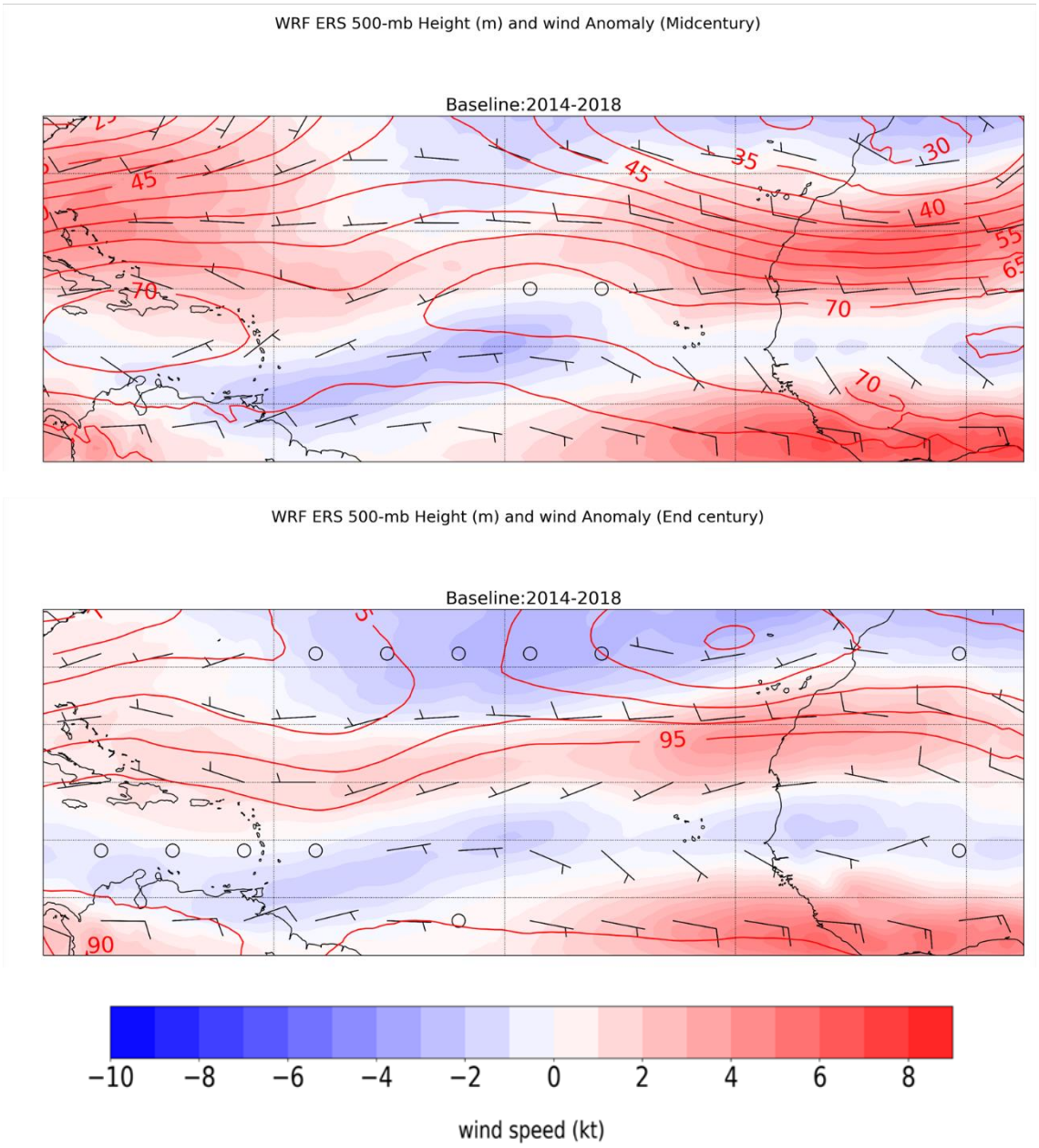

Figure B6. ERS 500 hPa future anomalies. Positive values indicate higher values in the future period.

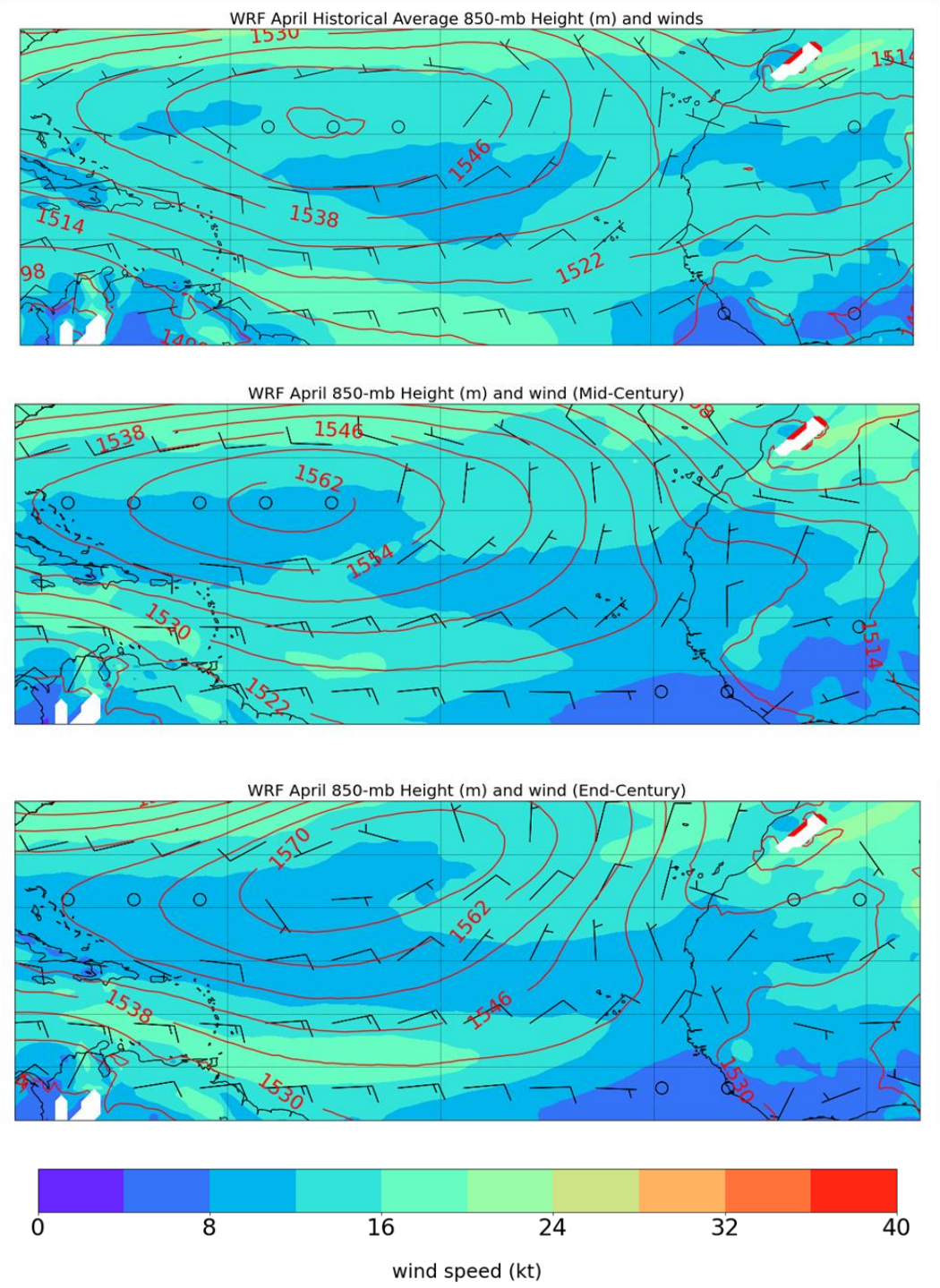

Figure B7. April 850 hPa pressure level heights, wind speed and wind direction for the Historical, IC, and EC.

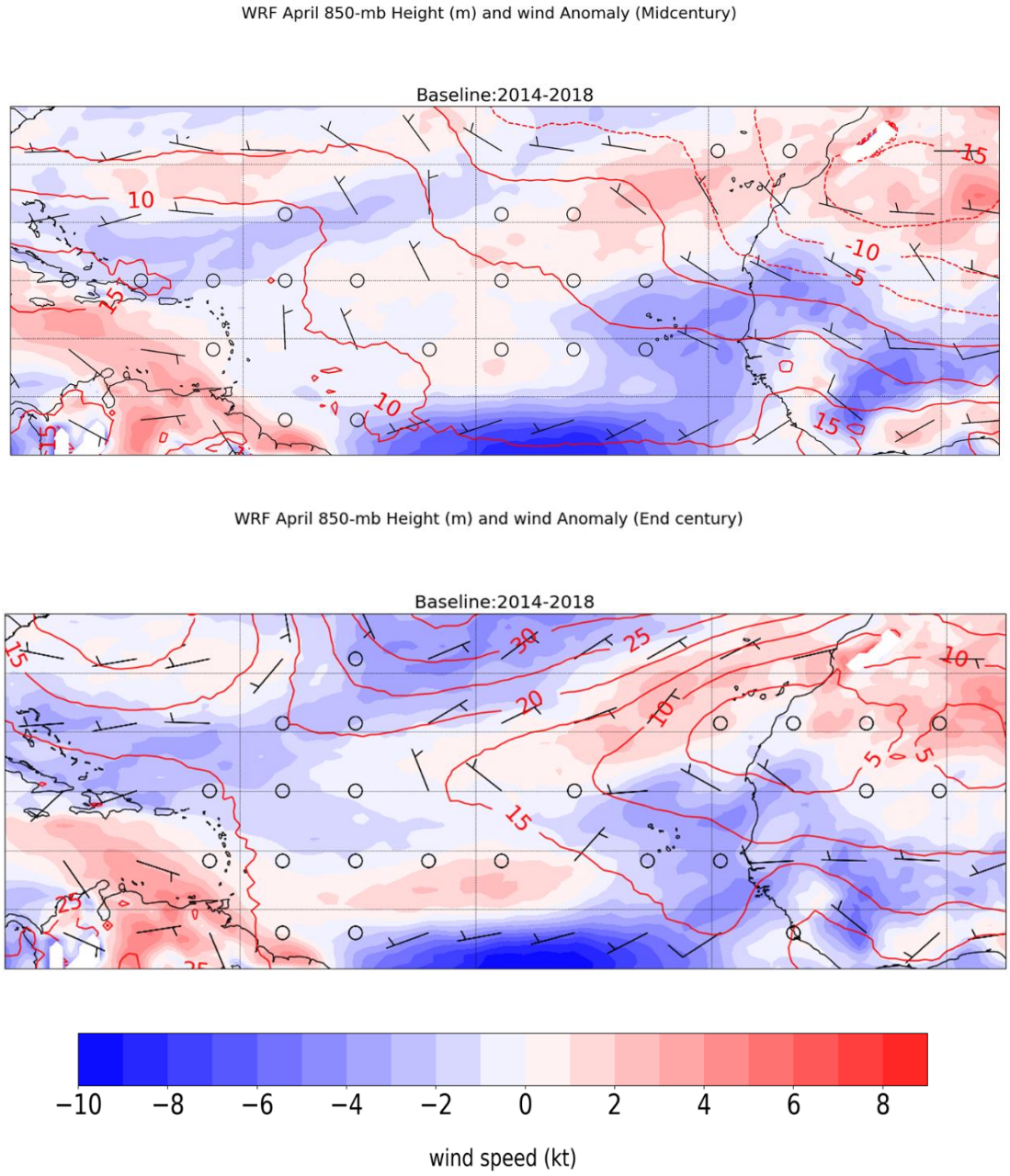

Figure B8. April 850 hPa future anomalies. Positive values indicate higher values in the future period.

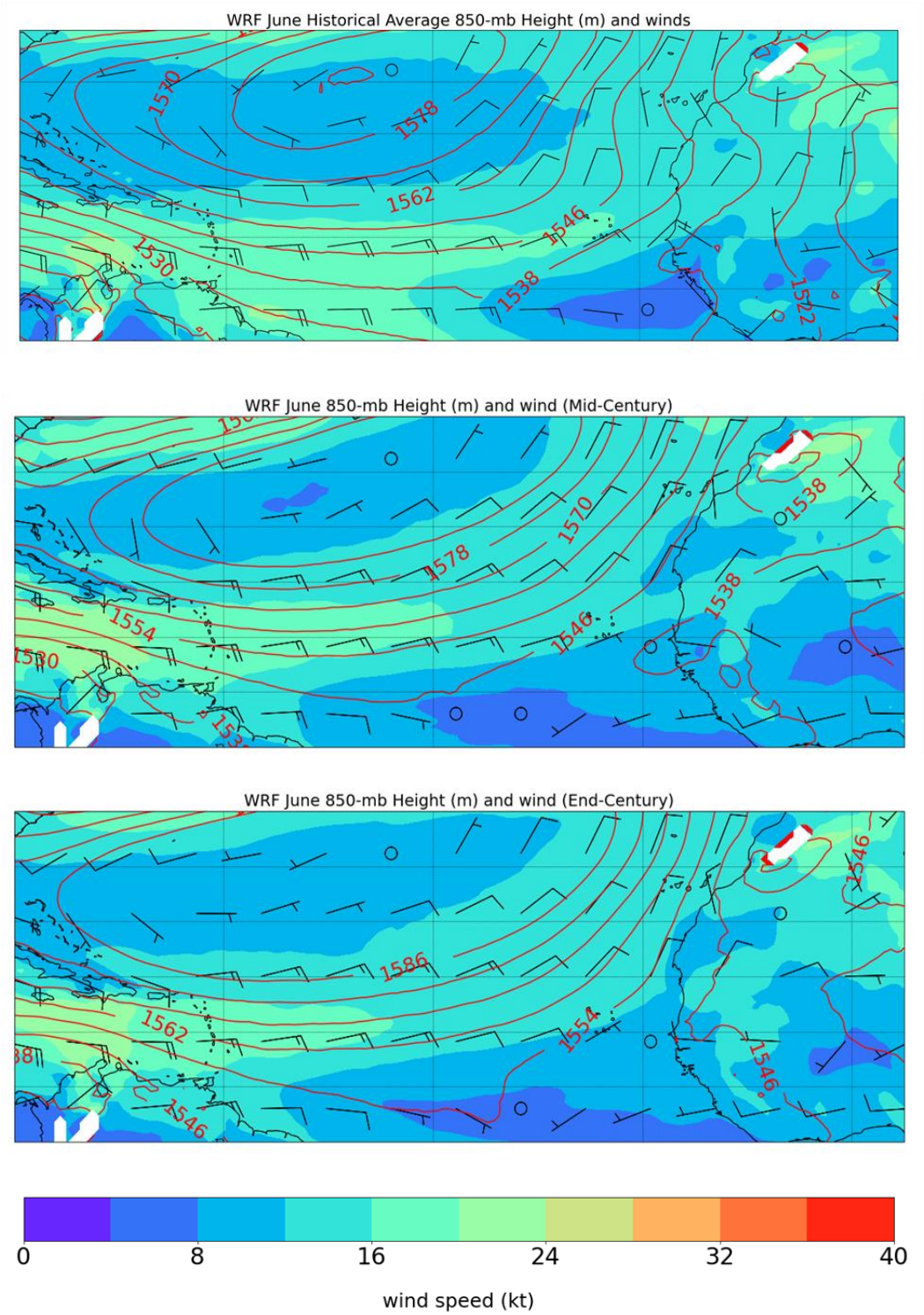

Figure B9. June 850 hPa pressure level heights, wind speed and wind direction for the Historical, IC, and EC.

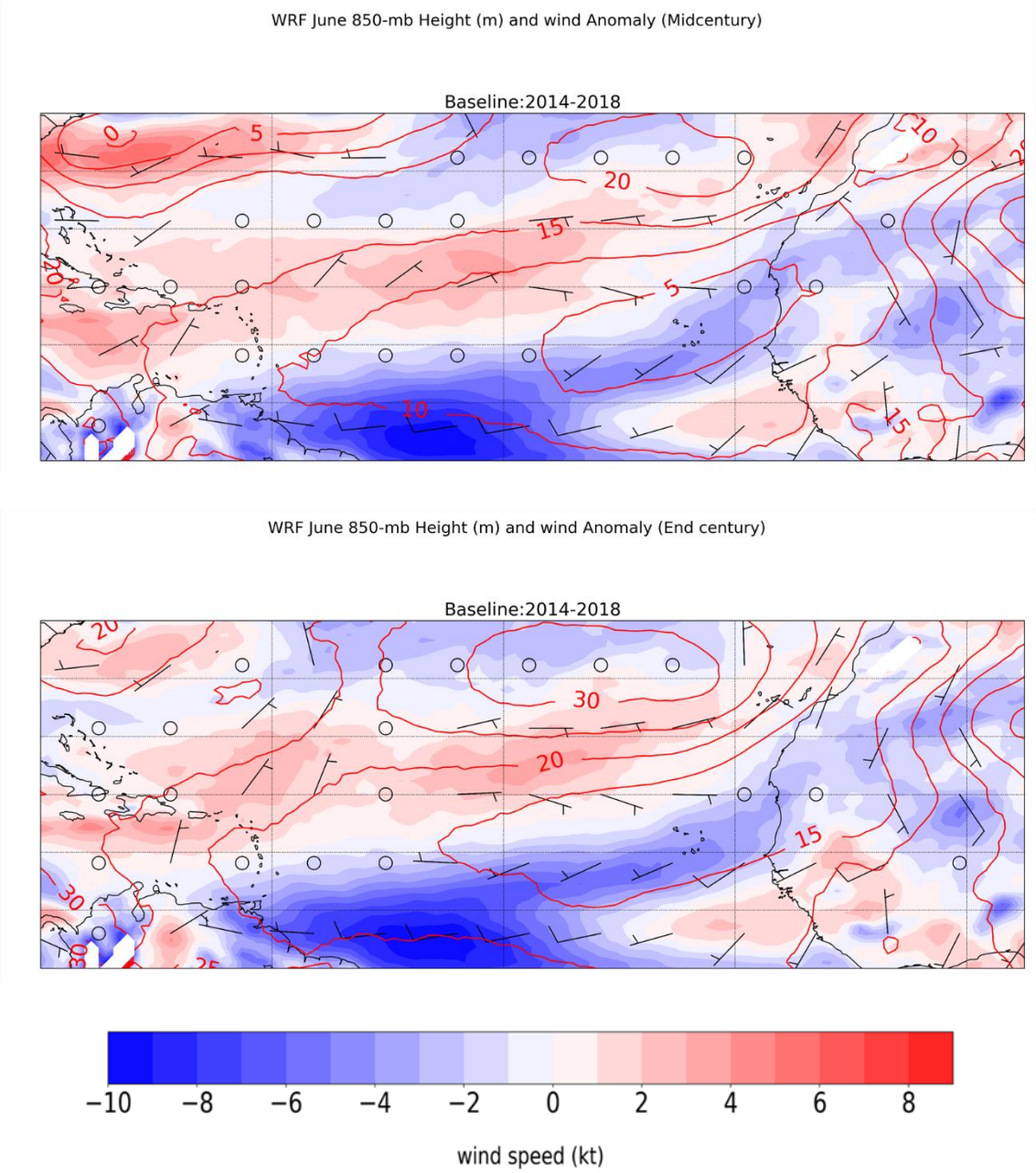

Figure B10. June 850 hPa future anomalies. Positive values indicate higher values in the future period.

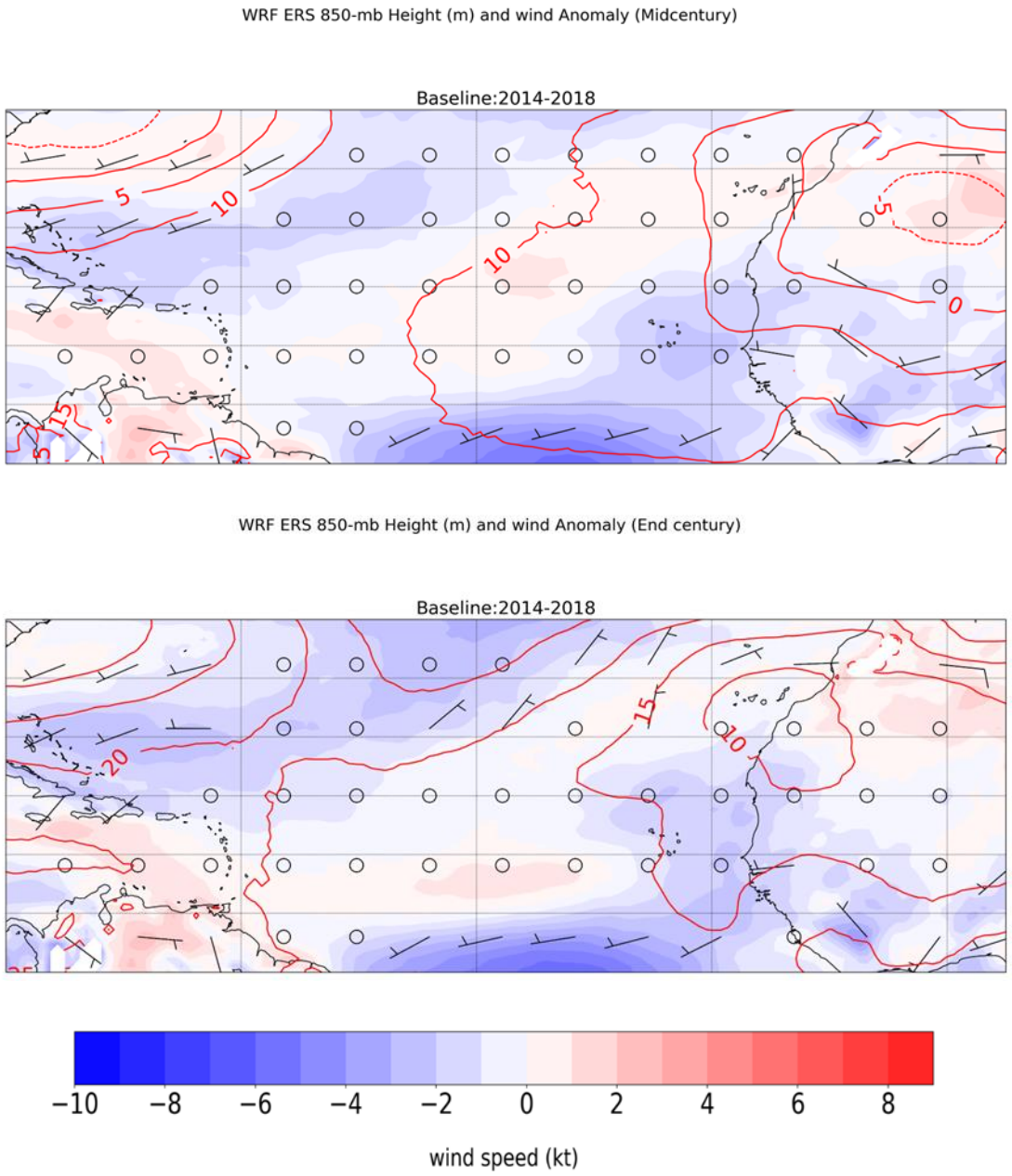

Figure B11. ERS 850 hPa future anomalies. Positive values indicate higher values in the future period.

Appendix C: WRF ERS and Dust Season AOD Timeseries

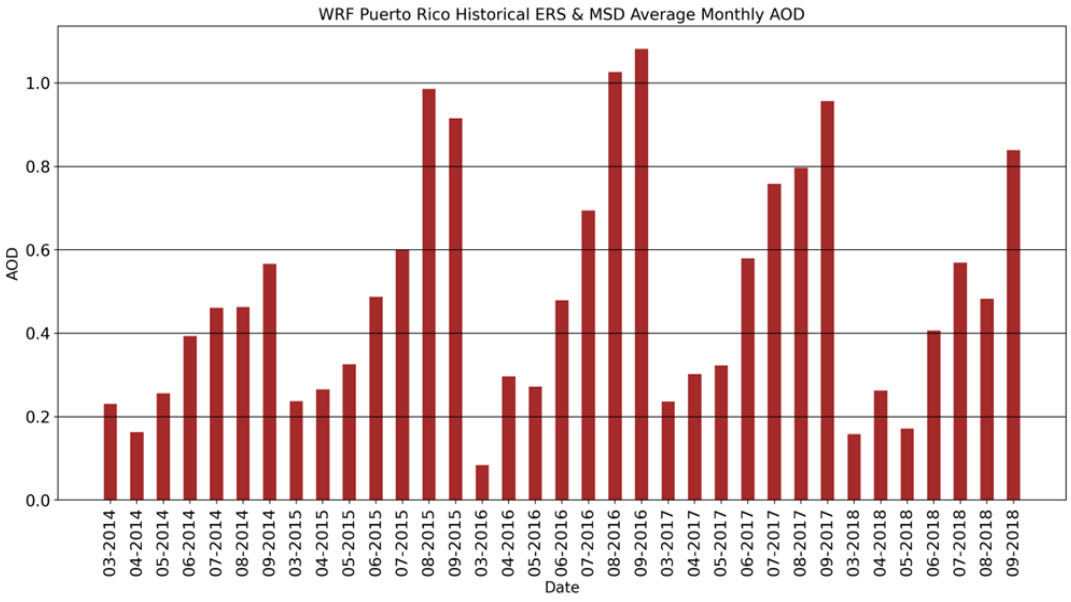

Figure C1. Monthly mean AOD for the Historical period during the ERS season and MSD months of March through September.

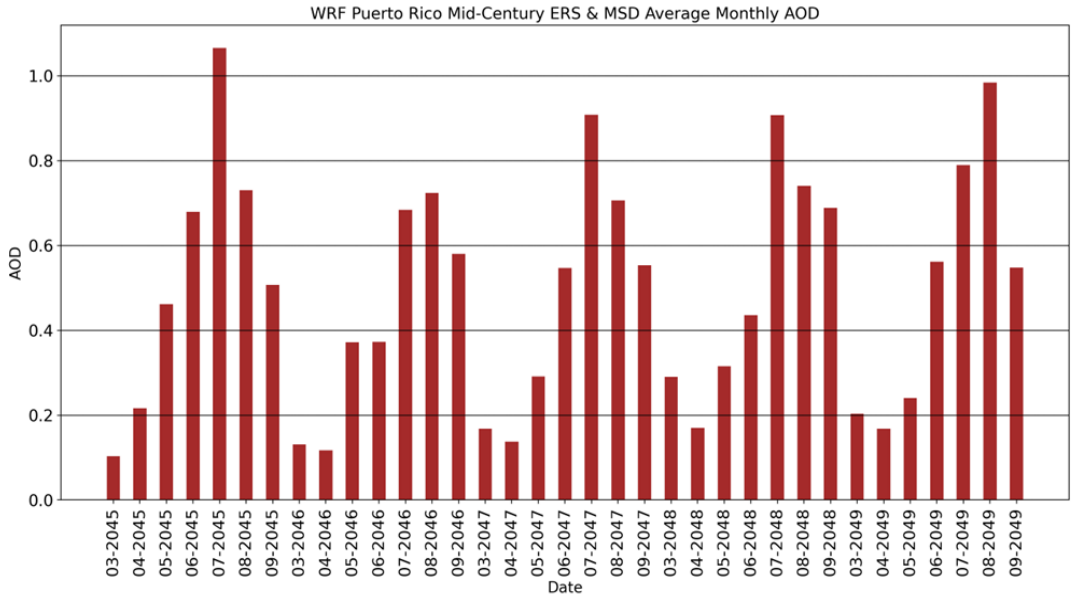

Figure C2. Monthly mean AOD for the mid-century period during the ERS season and MSD months of March through September

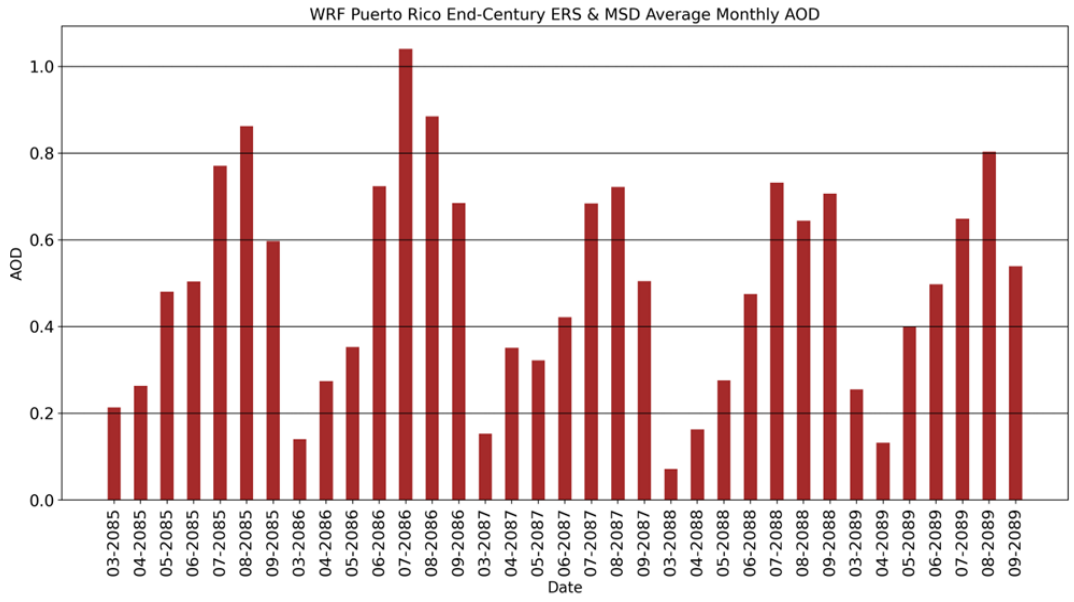

Figure C3. Monthly mean AOD for the end-century period during the ERS season and MSD months of March through September

Appendix D: Aerosol Optical Depth

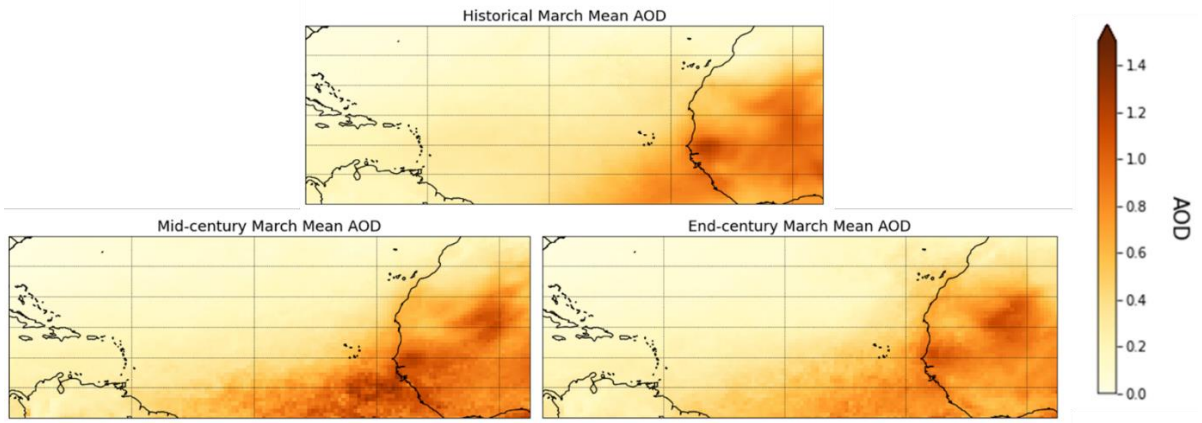

Figure D1. March averaged AOD for the historical, mid-century and end century periods.

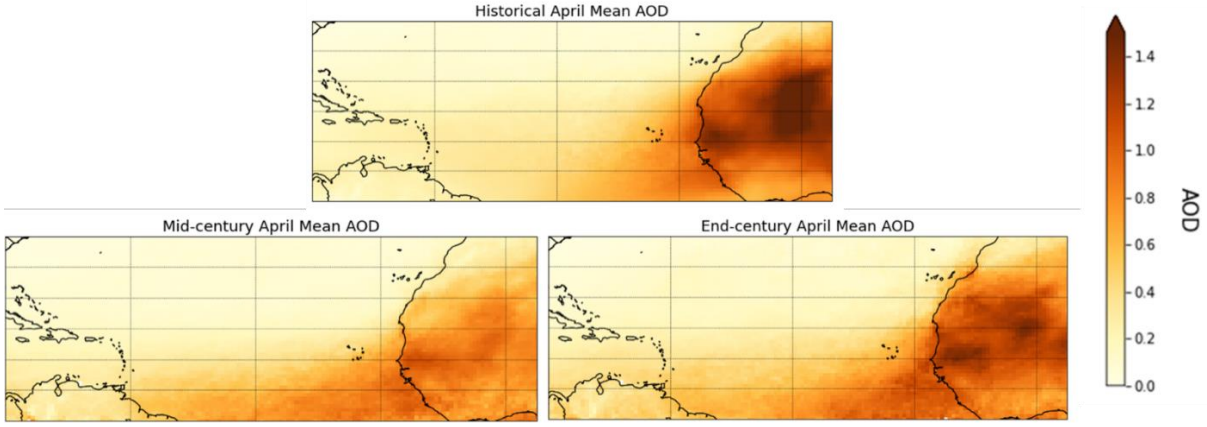

Figure D2. April averaged AOD for the historical, mid-century and end century periods.

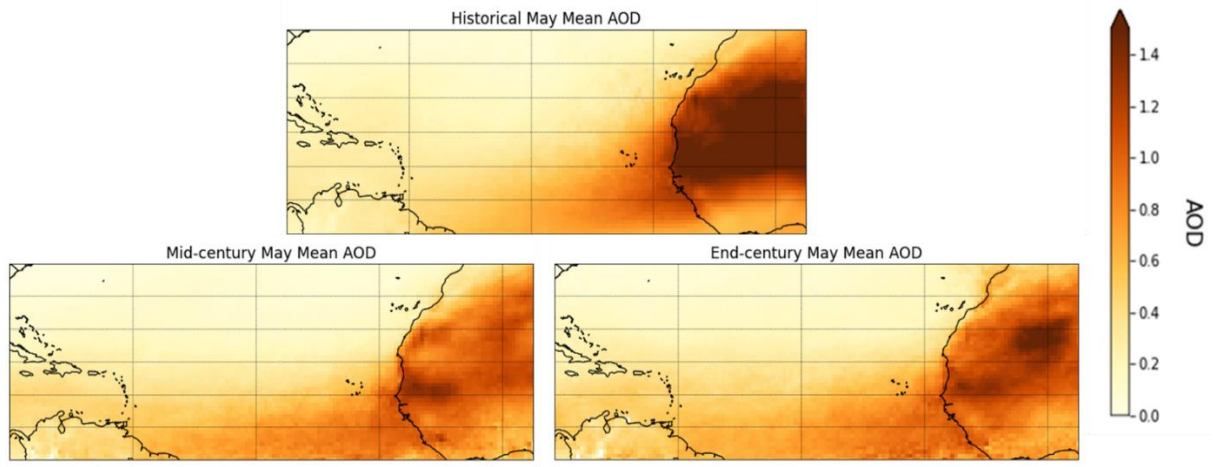

Figure D3. May averaged AOD for the historical, mid-century and end century periods.

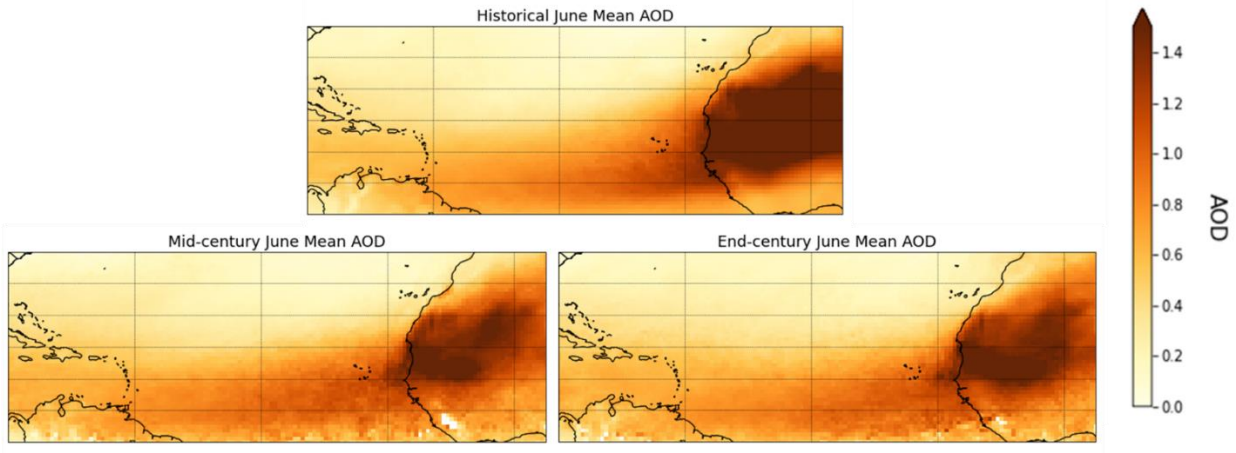

Figure D4. June averaged AOD for the historical, mid-century and end century periods.

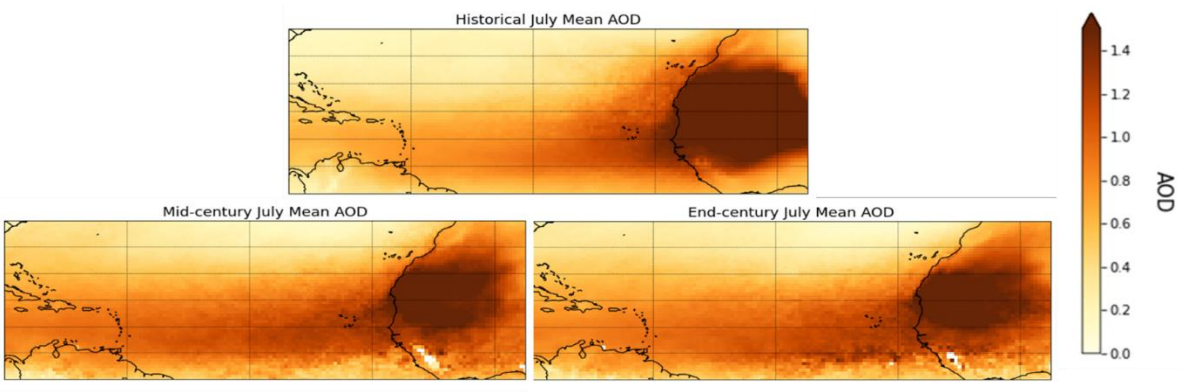

Figure D5. July averaged AOD for the historical, mid-century and end century periods.

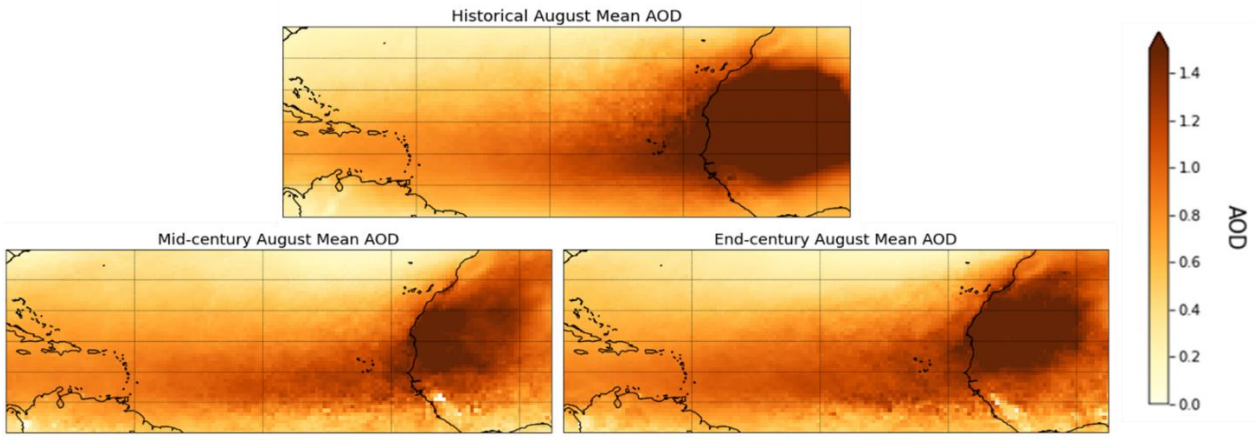

Figure D6. August averaged AOD for the historical, mid-century and end century periods.

Appendix E: Rainfall

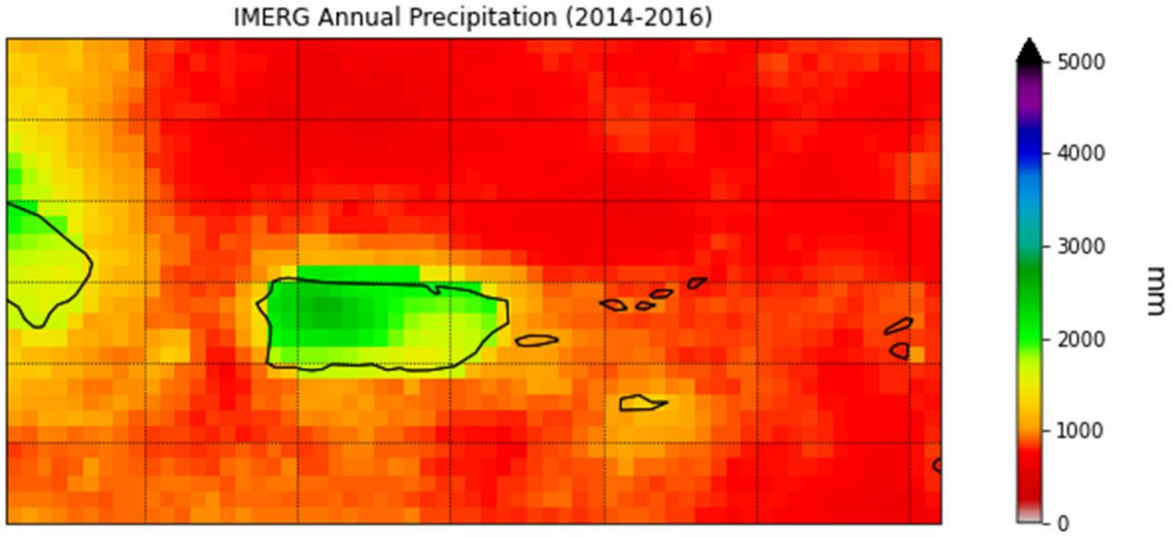

Figure E1. IMERG annual rainfall for January 2014 through December 2016 (mm/yr).

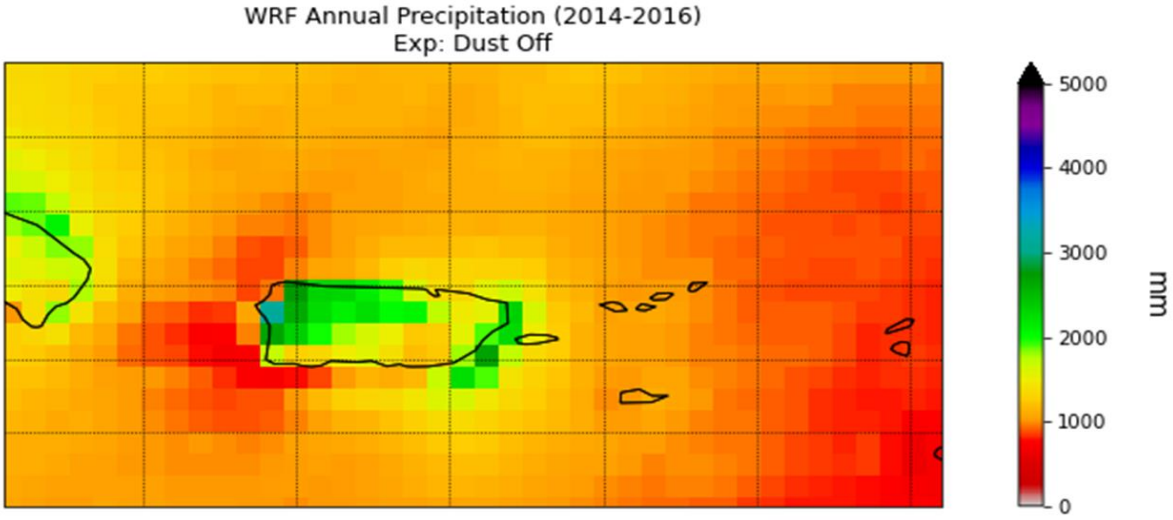

Figure E2. WRF ‘dust off’ simulation annual H rainfall (mm/yr).

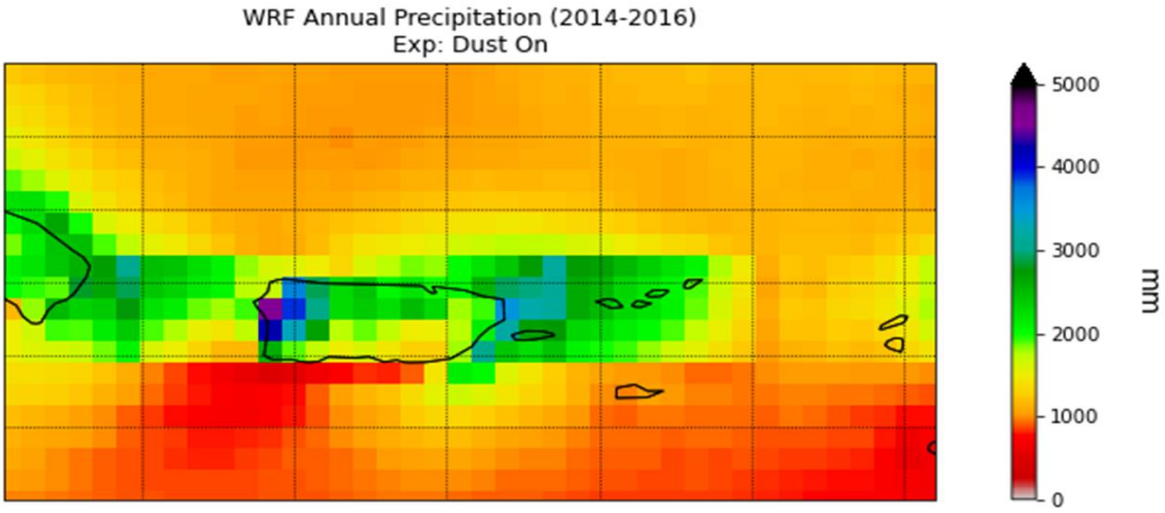

Figure E3. WRF ‘dust on’ simulation annual H rainfall (mm/yr).

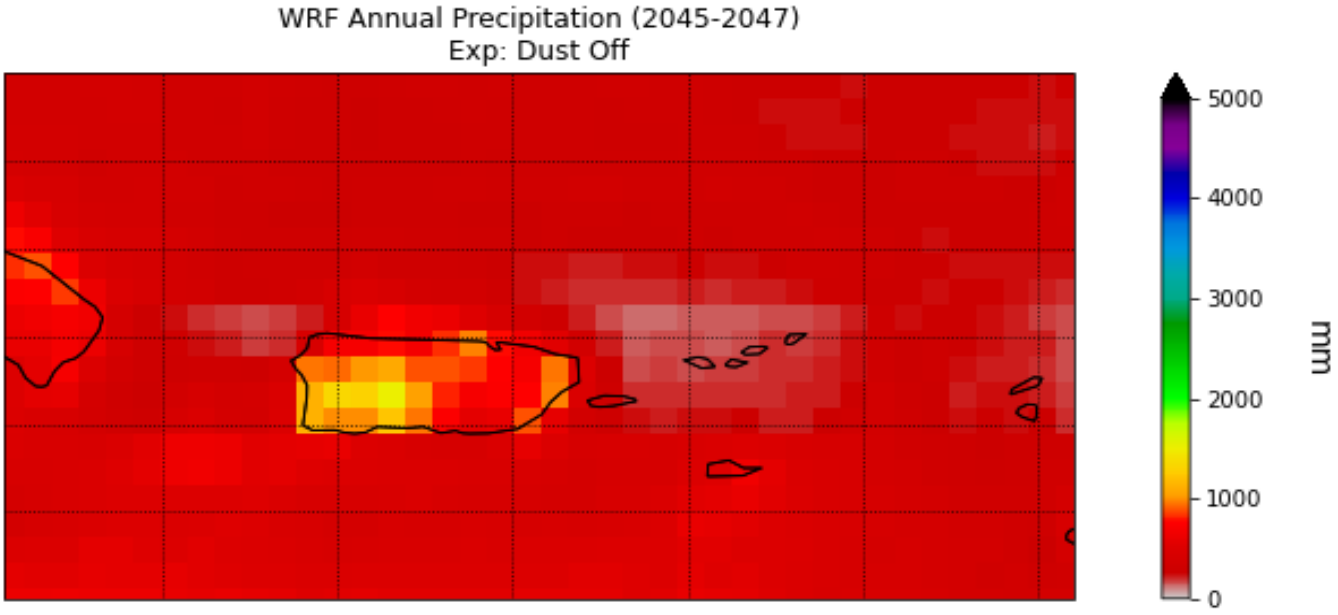

Figure E4. WRF ‘dust off’ simulation annual MC rainfall (mm/yr).

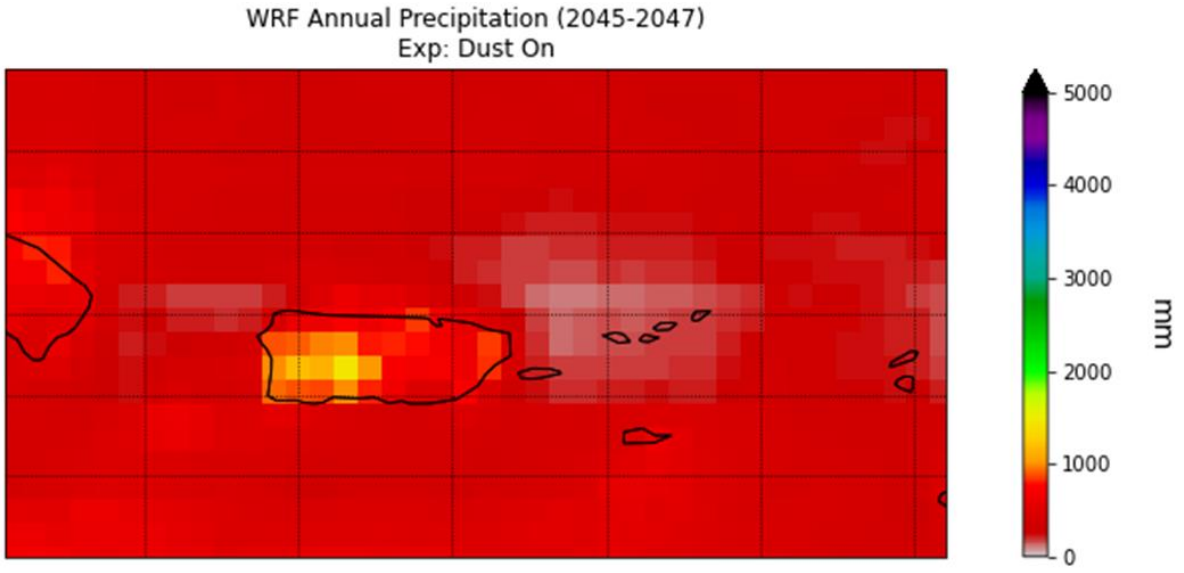

Figure E5. WRF ‘dust on’ simulation annual MC rainfall (mm/yr).

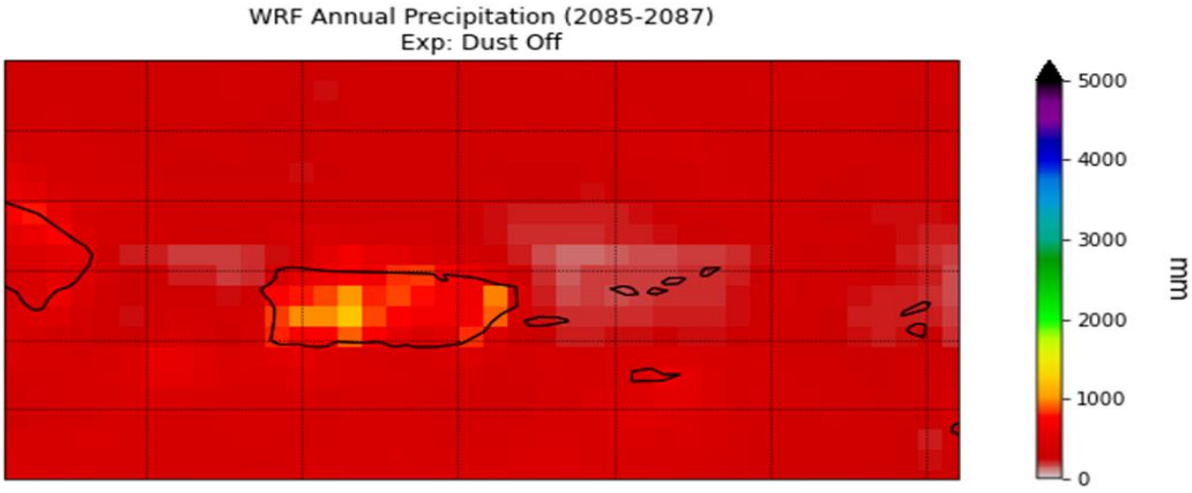

Figure E6. WRF ‘dust off’ simulation annual EC rainfall (mm/yr).

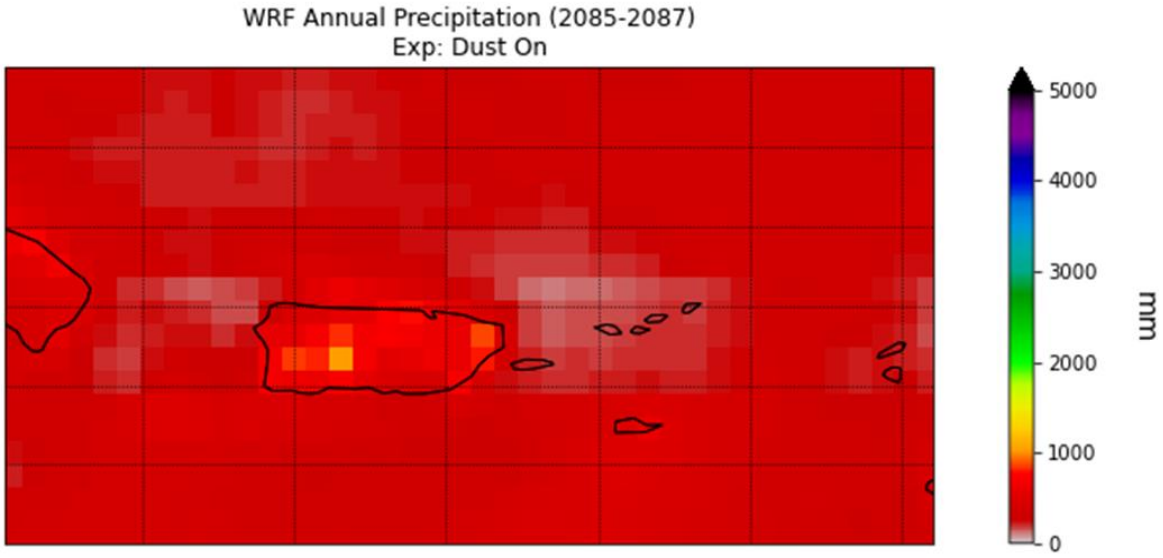

Figure E7. WRF ‘dust on’ simulation annual EC rainfall (mm/yr).